ANNALS OF GEOPHYSICS, 65, 6, SE643, 2022; doi:10.4401/ag-8387
OPEN ACCESS

A refined catalogue of focal mechanisms for the Intra-Carpathian region of Romania: implications for the stress field and seismogenic features assessment

Eugen Oros[*,1], Mihaela Popa[1,2], Paulescu Daniel[1], Anica Otilia Placinta[1], Cristian Ghita[1]

(1) National Institute for Earth Physics, Calugareni Street, No. 12, Magurele 077125, Ilfov, Romania
(2) Academy of Romanian Scientists, Ilfov Street, No. 3, sector 5, 030167 Bucharest, Romania

Article history: received November 12, 2019; accepted May 5, 2022

Abstract

We present a refined and the most complete catalogue of the focal mechanisms for the Intra-Carpathian region of Romania. It contains the high-quality solutions computed for 1217 earthquakes recorded between 1909 and 2018. Primary data gathered from the original seismograms and seismic bulletins have been used to compute the source parameters and focal mechanisms solutions. The focal mechanisms have been obtained using the HASH method by the polarities and S/P amplitudes ratios inversion. Our catalogue provides data necessary for the investigation of the contemporary stress field at different scales with high spatial and temporal resolution. We determined the stress field characteristics through formal inversion of focal mechanisms and also computed the reactivation potential of the active fault systems using the Win-Tensor program. The stress field is heterogeneous, with SHmax significantly deviating from the first-order stress field direction and also with strong local variations in the stress regime.

Keywords: Focal Mechanisms; Seismological data; Stress, Seismotectonics; Historical seismograms

1. Introduction

Earthquake focal mechanism solutions (FMS) are geometric/mathematical expressions of seismic faulting and are unique sources of *in situ* information that describe the rupture processes during an earthquake. Analyzed together with all available geoinformation they can contribute fundamentally to the realistic modelling of the seismogenic structures including their reactivation potential assessment (slip-tendency, ST). To be effective, the catalogues of FMS have to contain a large diversity of mechanisms [Hardebeck and Hauksson, 2001] for which the information on their quality must be explicitly presented [Duputel et al., 2012]. One of the most important applications of focal mechanism catalogues is stress tensor estimation. Knowing the stress tensor, it is possible to predict the faults that are the most likely to be reactivated and the predominant type of faulting in a seismically active zone as a decisive step in the seismic hazard assessment.

Seismic monitoring of the Intra-Carpathian region of Romania (ICRR) has a long history. It started using the Bassart seismometer installed in 1889 in Bucharest, the Konkoly-Vicentini seismograph installed in Timisoara in 1901-1902 and the setting up of seismic stations in Cluj and Cernauti [Oros, 2011; Popa et al., 2015; Radulescu, 2009; Toth et al., 2018 and references therein]. Today a network with more than one hundred stations (Figure 1) operates in real-time [Popa et al., 2015]. The increase in the station number and the use of modern digital data acquisition and processing technologies over the past decades led to improved detection and localization capabilities for smaller seismic events with a major impact on the determination of reliable and stable FMS.

The FMS of crustal earthquakes in Romania were determined and published over time in several articles, research reports, theses and seismic bulletins, etc. [Cornea et al., 1980, Malita and Radulescu, 2010; Oros et al., 2008b; Oros, 2011; 2013; 2014, Placinta et al., 2016, Popa et al., 2018, Radulian et al., 1996; 1999; 2018; Toth et al., 2018]. However, only a few studies focused on crustal stress field investigation in the ICRR using modern techniques that assess the stress tensor and stress regime by focal mechanism inversion [e.g. Bada et al., 2007; Oros, 2011]. Other authors used in the stress tensor inversion both focal mechanisms and geological/borehole data to predict the smoothed stress pattern [e.g. Muller et al., 2010; Heidbach et al., 2018 and references therein]. Zugravescu et al. [2005] used only borehole stress indicators to describe the stress orientation in the Transylvanian Depression.

In this paper we present a new catalogue of FMS determined for the crustal earthquakes recorded between 1900 and 2018 in the study region. The FMSs have been obtained through an inversion of polarities and the S/P amplitude ratio. For most of the events imported from the literature, source parameters (location, focal depth, magnitude) were revised using, when possible, primary data collected from seismograms or seismic bulletins. The final catalogue also contains the FMS of the earthquakes that occurred during the pre-digital instrumental period (1900-1980). We performed a detailed analysis and modelling of the contemporary stress field and we estimated the reactivation potential of geological structures, including the most likely faulting style.

2. Tectonic and seismotectonic features

The ICRR is located in the eastern sector of the Carpatho-Pannonian Basin where two micro-plates developed, namely Alpaca and Tisa-Dacia, separated by a large Paleogene-Early Miocene shear zone ("Mid-Hungarian Zone") [Sandulescu, 1984; Schmid et al., 2008 and references therein]. The limits of ICRR are defined through the crustal and geodynamic block architecture, the Neogene volcanic chain from Eastern Carpathians and the neotectonic like-grabens structures of the Pannonian Basin [Sperner et al., 2004, Polonic, 1985; Sandulescu, 1984, Zugravescu and Polonic, 1997]. Several morpho-structures developed within ICRR, namely the Transylvanian and Pannonian Depression (eastern border), Apuseni Mountains and large areas of Eastern and Southern Carpathians. The pre-Alpine basement entities are described as Dacides, Transylvanides and Moldavides [Sandulescu, 1984]. They are made up of nappes, suture zones, closed rifts and magmatic bodies locally covered by post-tectonic sedimentary formations. Many fault systems, successively reactivated during their Alpine history under different stress conditions fragmented the region controlling its kinematic and geodynamic evolution (Figure 1). The major faults that could support the kinematic evolution of the region are the North and South Transylvania faults (NTF and STF), Puini Thrust Fault (PTF), Intramoesian Fault (IMF), South Carpathian Fault (SCF), Western Fault (WF) and Cerna-Jiu Fault (CJF) [Linzer et al., 1998; Sandulescu, 1984].

Three Alpine tectonic events have been identified in the region (for details see Linzer et al., 1998 and references therein): 1) NE to ENE Paleogene-Middle Miocene contraction that caused right-lateral curved strike-slip faults in the South Carpathians (WF, CJF and SCF system), 2) fan-shaped orientation of the contraction directions that caused mainly thrusting of the nappes in the Eastern and Southern Carpathians (Middle Miocene-Pliocene): NE to ENE orientation in the northern Eastern Carpathians and ESE to SE orientation in the southern Eastern Carpathians and the Southern Carpathians. In the CM zone, local blocks rotate up to 90° accompanied by NW-SE-oriented extension events, 3) Quaternary (Pleistocene to Holocene) E-W extension and N-S contraction characterized by left-lateral strike-slip faulting on major segments of the NTF system (Dragos Voda and Somes faults; Polonic, [1985]), normal faulting in the southern Eastern Carpathian (Brasov Basin) and right-lateral faulting in transtensive conditions in the South Carpathian (WF, CJF, SCF, IMF). A contraction WNW-ESE post-Badenian has been recorded in the southwestern part of the North of Apuseni Mts and in the Transylvanian Basin where NS-oriented thrust faults have been reactivated (e.g. PTF). On the western border of the Apuseni Mts, like-graben structures developed under basinal inversion conditions with NW-SE-oriented extension (Pannonian).

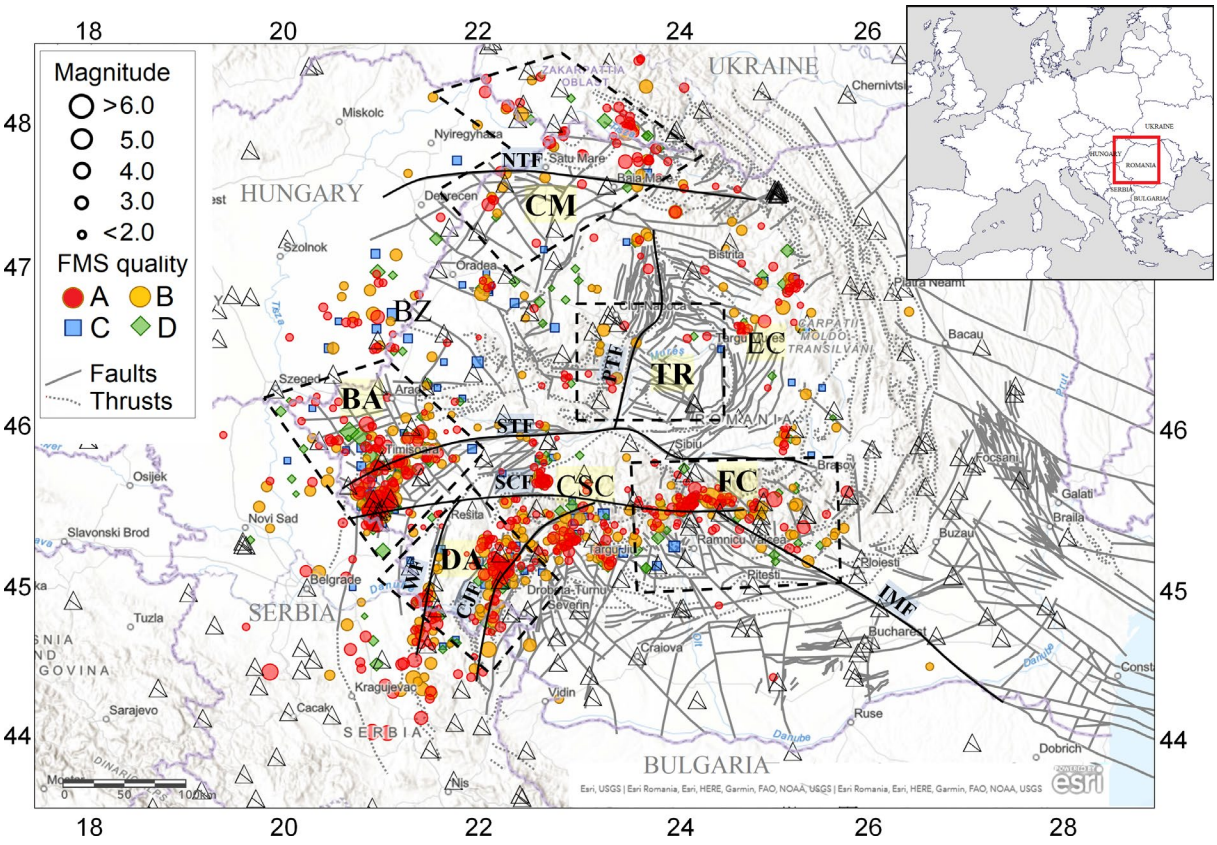

Figure 1. Map of focal mechanisms according to quality and moment magnitude, Mw (N = 1217, 1901-2018). Triangles are seismic stations. The dashed line polygons border the seismogenic zones defined by Popa et al., [2015]: FC: Fagaras-Campulung, DA: Danube Zone, BA: Banat Zone, CM: Crisana-Maramures, TD: Transylvania. Grey lines are faults [after Linzer et al., 1998; Sandulescu, 1984; Zugravescu and Polonic, 1997]: NTF: North Transylvania Fault, PTF: Puini Thrust Fault, STF: South Transylvania Fault, SCF: South Carpathian Fault, CJF: Cerna-Jiu Fault, IMF: Intramoesian Fault. Zones with high seismic activity: Bekes-Zarand basin (BZ), Eastern Carpathians-Neogene Volcanic Area (EC), South Carpathians-central area (CSC).

The present-day regional stress and ongoing deformations are controlled by the complex interaction of plate boundary as the main first-order stress source ("Adria-push") and intra-plate forces (elevated topography, crustal and lithospheric inhomogeneities, thermal stress, active major faults) [Bada et al., 1998; 2007; Muller et al., 2010].

Moreover, the active NW-SE compression at the Vrancea zone, the slight compression from the Bohemian Massif and the presence of the stable Moesian Platform could induce additional stresses in the North and East-South East [Bada et al., 1998]. The smoothed model of the tectonic stress in the study region shows a NE-SW-oriented SHmax in the western half that changes progressively towards E-W and roughly ESE-WNW in the centre and eastern half, respectively [Bada et al., 1988; 2007; Heidbach et al., 2018].

The crustal seismicity in Romania shows a dispersed pattern. However, several areas with well-defined high seismic activity related to the major fault systems and the contact between tectonic units were described as seismogenic sources by Radulian et al. [2000] (Figure 1). ICRR experienced several significant crustal earthquakes [e.g. Oncescu et al., 1999; Oros, 2011]: 1) at the tectonic contact area between Tisa Microplate and Mid Hungarian Zone where large like-graben structures develop and the NTF controls their neotectonic evolution (Ms = 6.4, November 26, 1829; Ms = 6.3, October 15, 1834) and 2) In the South, at the intersection between the SCF and IMF (January 26, 1916, Ms = 6.4) and along to CJF (July 18, 1991, Mw = 5.7) [Oros, 2011; Oros et al., 2019a]. Moderate events, but with heavy macroseismic effects, have been recorded 1) in Transylvania Basin probably associated with the STF and its intersection with NS-oriented reverse PTF (August 17, 1569, Mw = 5.8; October 3, 1880, Mw = 5.4) and 2) on the southeastern border of the Pannonian Basin within a large area of SCF-STF intersection (July 12, 1991, Mw = 5.6) and along to WF (October 10, 1879, Mw = 5.8).

3. Data and methods

We gathered the data from 1) catalogues of earthquakes [Oncescu et al., 1999, updated version at www.infp.ro; Oros et al., 2008a], 2) studies, research reports, articles containing FMS [Oros et al., 2008b; Popa et a., 2018; Radulian et al., 2002; 2018 and references therein]; 3) seismic bulletins (ISC-www.isc.ac.uk, EMSC-www.emsc-csem.org, GeoRisk-MTA GGKI-www.georisk.hu), 4) seismograms recorded by NIEP with permanent and temporary stations (e.g. the July and December 1991 campaign in western Romania, Oros [2011]) and as a partner in international programs (e.g. South Carpathian Project 2009-2011, Ren et al. [2013]; Geofon-https://geofon.gfzpotsdam.de), 5) macroseismic maps (e.g. Oros, 2011] and references therein; NIEP Technical Reports]. We also used the scanned bulletins and seismograms obtained through the EuroSeismos project [Ferrari and Pino, 2003; http://storing.rm.ingv.it/es_web] for the major earthquakes that occurred during the pre-1960 and the pre-digital early instrumental (1960-1980) periods. This collection was completed with seismograms and bulletins stored in the database of the SISMOS project [Michelini et al., 2005] accessible at http://sismos.rm.ingv.it/index.php and in the NIEP archive [Paulescu et al., 2016] accessible at www.archive.infp.ro. The seismograms have been digitized by Oros [2011] and Oros et al. [2019a] using the Teseo2 program [Pintore et al., 2005].

First, we compiled a work catalogue with over 6000 crustal earthquakes recorded since 1900 (Mw = 0.2-6.4, depth = 1.0-60.4 km). Then, we eliminated all possible industrial explosions by applying the method of the ratio of the number of events that occurred in the day- and nighttime which assumes that industrial explosions occur during the day at about the same time and in the same areas. We eliminated these events after a careful analysis of seismograms regarding the main characteristics of the explosions such as monochromatic spectrograms, Rayleigh waves at small epicentre distances, positive polarities for all vertical components, the similarity of waveforms recorded at the same stations in the same locations and $Mw \leq 2.5$ [e.g. Allmann et al., 2008, Giardini et al., 2004; Kulhanek, 2002; Oros, 2011; Ursino et al., 2001]. We are aware that the decontaminated catalogue still contains possible explosions and some of the tectonic earthquakes are eliminated. In the end, we eliminated the events for which 1) we did not have at least 6 polarities when we used data obtained from analogue recordings or bulletins and 2) at least 4 polarities and one S/P ratio for digital data. The travel times and polarities of the P waves have been picked on unfiltered waveforms (vertical components) except those with signal/noise ratio $S/N > 2.5$ for which we applied very carefully filters, such as band-pass filter, Butterworth 4 poles at frequencies higher than 1 Hz and lower than corner frequency [Diehl and Kissling, 2007; Hardebeck and Shearer, 2003; Ottemoller et al., 2014 and references therein]. The amplitudes were measured in 2-second windows after the onset of the P and S direct waves.

The final catalogue contains reliable data on 1217 earthquakes recorded between 1901 and 2018 with Mw = 1.1-6.4 and focal depths h = 1.1-57.8 km (Figure 1 and Figure 2a, b). Most earthquakes occurred in the upper crust ($h < 20$ km) and have $Mw < 3.5$. Only 20 events are deeper ($h > 20$ km) and are located in the Southern Carpathians. The threshold of location magnitude decreased significantly after 2000 (Figure 2c) when S/P ratios are available for broadband 3 components recordings. The number of polarities and S/P ratios used in this paper (No_Pol = 15369, No_SP ratios = 2134) is higher during the 1991 seismic sequence that occurred in the western part of Romania and during the South Carpathians International Project (2009-2011) when the monitoring campaigns used networks of mobile stations (Figure 2d).

3.1 Earthquake relocation

We relocated the independent earthquakes using Seisan software [Ottemoller et al., 2014]. It accepts multiple phases and allows the interactive use of constraints, such as the variable weights and the time difference between the arrivals of P and S or P and Lg waves (S/L-P times). For grouped earthquakes, we used the Joint Hypocentral Determination, JHD method [Pujol, 2000].

The earthquakes recorded before 1960 have been relocated using, as a matter of priority, the travel time of the surface waves that are better recorded on horizontal components of the mechanical and electromagnetic instruments, and the S/L-P times to compensate for uncorrected time data. Their locations were validated by macroseismic methods calibrated by Oros et al. [2019, 2019b].

The number of stations used to relocate the events ranges from N = 4 (minimum one S-wave arrival) up to N = 190. We obtained RMS = 0.1-2.1 s (92% RMS < 0.6 s, over 50% RMS < 0.4) and station gap = 15°-303° (94% gap < 180°, 55% gap ≤ 90°). The highest RMS and gap values have been obtained when we used analogue data and for

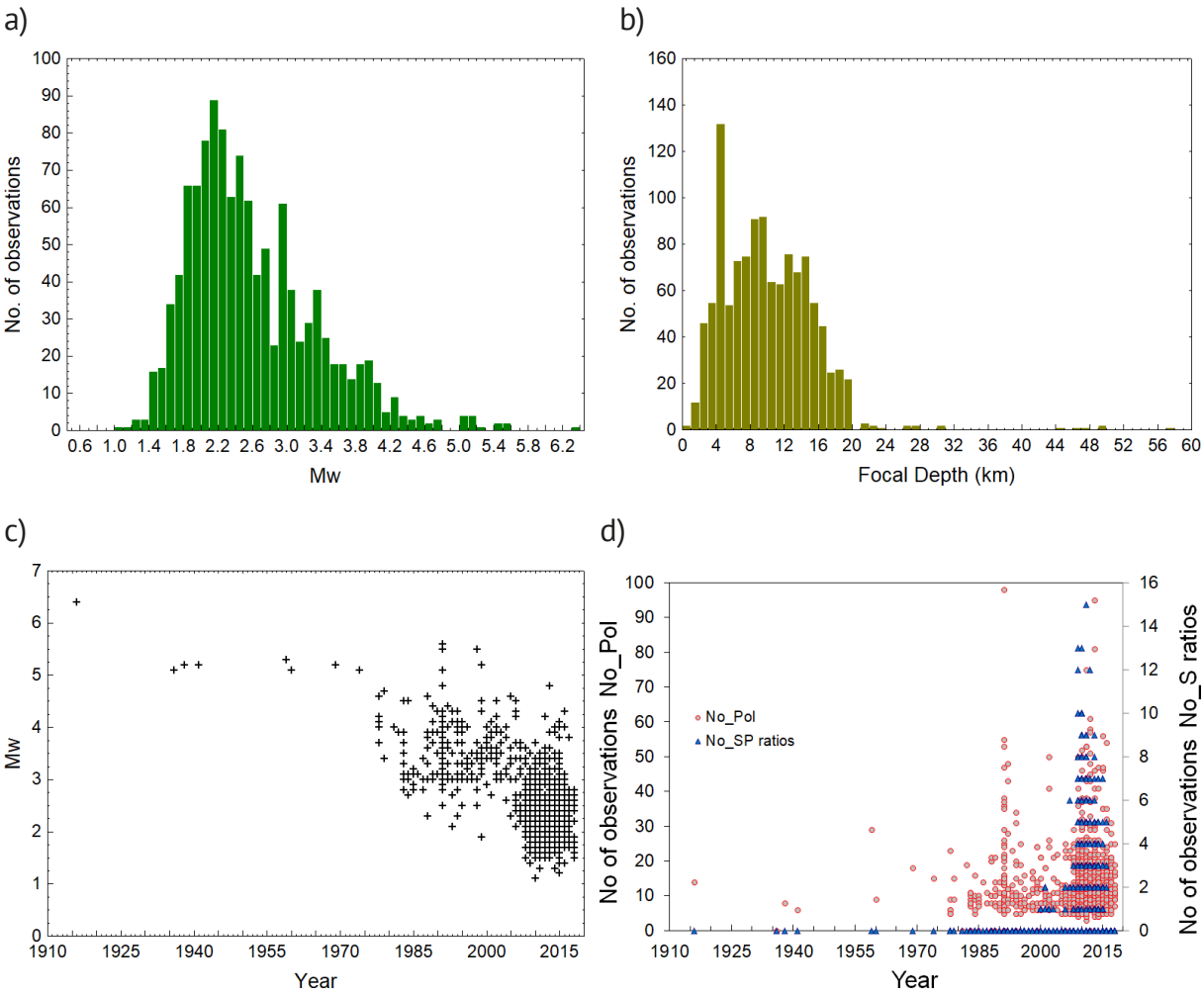

Figure 2. The earthquakes selected to determine the focal mechanism solutions. Histograms of magnitude (a), depth (b), Mw = f(time) (c) and the number of polarities (No_Pol) and S/P ratios (No_SP ratios) (d).

the events located at the edges of the network. For a significant number of events, RMS decreased by using correctly identified phases versus the original ones collected from bulletins. Our locations are of good quality if we consider the RMS, GAP and average localization errors, i.e. err_latitude = 2.5 km ± 1.8 km, err_longitude = 3.5 km ± 1.8 km, err_depth = 0.4h km ± 0.4 km, where h is the absolute depth value.

3.2 Magnitude

The moment magnitude Mw was estimated using the scalar seismic moment method implemented in the Seisan package or by conversion to Mw of different types of magnitudes and macroseismic data. For historical earthquakes, we applied the empirical formulae which relate Mw to isoseismal area, macroseismic intensities, Ii, epicentral or maximal macroseismic intensity, Io. These relations have been calibrated by Oros et al. [2017; 2019, 2019a]. Conversions Mw = f(Ms, mb) were made using the procedure of Oncescu et al. (1999). For most events we applied our new conversion relationships to Mw of local (ML) and coda (Mc) magnitudes:

$$Mw = 0.030ML^2 + 0.612ML + 1.026, N = 1096, R^2 = 0.862, ML = 0.2 - 6.0 \quad (1)$$

$$Mw = 0.146Mc^2 - 0.17Mc + 1.758, N = 768, R^2 = 0.810, Mc = 1.0 - 6.0 \quad (2)$$

3.3 Focal mechanism estimation

FMSs are defined by the geometry of two nodal planes (the strike, dip of fault plane, NP1 and auxiliary plane, NP2), the direction of slip vector or displacement of the hanging wall relative to the foot-wall (rake angle) and the azimuth and plunge of the three principal axes defining the moment tensor (P axis-compression, T axis-tension or extension, B axis-null axis). They are determined by methods based on the radiation pattern and using the distribution of observation data on the focal sphere. The most common methods use the inversion of the P-wave polarities (polarities) [Khatri, 1973]. More robust FMS are obtained by adding S/P amplitude (S/P ratios) [Kisslinger et al., 1981, Snoke et al., 1984; Hardebeck and Shearer, 2003; Reasenberg and Oppenheimer, 1985].

We computed FMSs using the HASH method [Hardebeck and Shearer, 2003] implemented in the Seisan package [Ottemoller et al., 2014]. This method employs S/P ratios apart from polarities, which increase the multitude of observations and consequently reduce the uncertainty of the solutions. Depending on the quality of the data we applied sometimes different procedures. One is based on the complementary inversion using different algorithms [e.g. FOCMEC, Snoke et al., 1984; FPFIT, Reasenberg and Oppenheimer, 1985] and the other one uses the full waveforms inversion, comparative analysis of synthetic waveforms with those observed or we introduced geological and macroseismic constraints.

For the earthquakes recorded with mechanical or electromagnetic instruments of low amplification and limited frequency range sensitivity (before 1980), we used scanned seismograms that have been processed by modern digital techniques (e.g. digitization, moment tensor inversion in the time domain). In Figure 3 we present the FMS

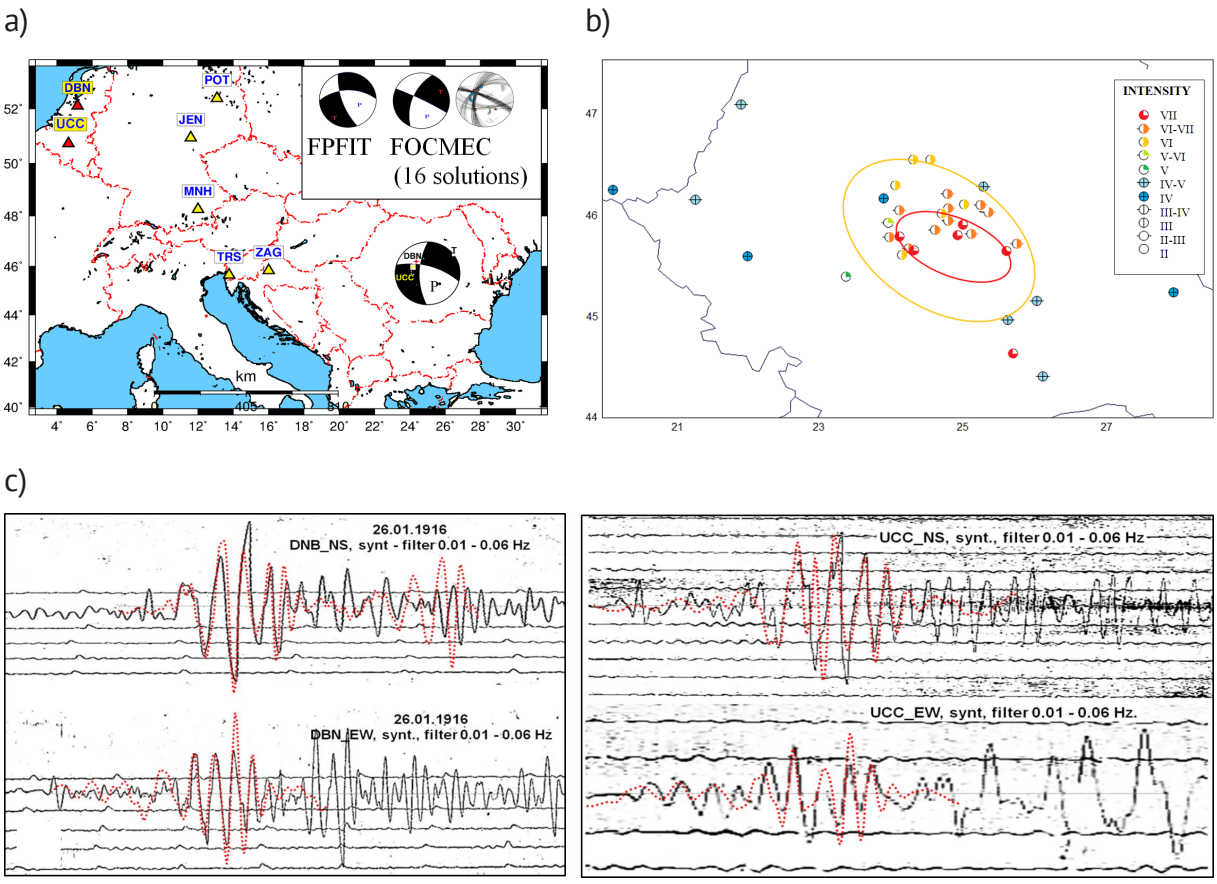

Figure 3. a) Focal mechanism solution computed for the Mw = 6.4, 26.01.1916 earthquake; red triangles are the stations used for the analysis of the waveforms; beach-ball symbols are FMS; *right upper corner*: focal mechanisms solutions computed using FOCMEC and FPFIT methods (red triangles are dilatations; blue circles are compressions). b) The macroseismic map (modified after Atanasiu [1961]); c) Comparison between observed (continuous black lines) and synthetic (red dotted lines) waveforms for De Bilt, Nederland (DBN) and Uccle Observatory, Belgium (UCC) stations. The synthetic waveforms are computed using the Seisan software [Ottemoller et al., 2014]; vertical scales have been adjusted to facilitate visual comparison.

computed for the Mw6.4, 26.01.1916 (Southern Carpathians) by inversion of polarities using three methods (N = 14 polarities, polarities gap Azp_gap = 147°, takeoff angle gap Tko_gap = 46°) (Figure 3a). The solutions are comparable, HASH: NP1 is 285°/65°/–149° and NP2: 181°/62°/–28°, FOCMEC: NP1 is 296°/85°/–144° and NP2: 202°/54°/–6.2°, FPFIT: NP1 is 269°/52°/–152° and NP2: 161°/68°/–41°. We computed synthetic waveforms for the HASH solution using Bouchon's method [1981], the velocity model ak135 (Kennet et al., 1995) and the attenuation factor Q = 400 [Malagnini et al., 2000] and filtered them with Butterwoth, bandpass, 4 poles filter and cutting frequencies of 0.01 and 0.06 Hz (Figure 3c). Then we compared them with those recorded at De Bilt and UCC stations (DBN, Netherland, Bosch horizontal pendulum, weight = 25 kg, To = 18.3 sec, Vo = 20, smocked paper, epicentral distance De = 1602 km; UCC, Belgium: Wiechert horizontal astatic seismograph, weigh = 1000 kg, To = 11.3 sec, Vo = 152, smocked paper, epicentral distance De = 1608 km). They are similar on both the onset and the content of the analyzed surface waves group, suggesting the accuracy and stability of the HASH solution. Furthermore, NP1 is oriented about NW-SE on the elongation direction of the maximum intensity isoseismal (Figure 3b) and follows the directions of the major faults.

When data about amplification, damping, free period, time corrections and drum speed were available, we determined FMS by full waveform inversion using digitized unrotated seismograms.

In Figure 4 we present the FMS determined for the 06.09.1936 (Mw = 5.1) earthquake that has been localized using data from 44 stations (Demax = 72°, Vladivostok station). We used the seismograms recorded by the Zagreb (ZAG), De Bilt (DBN) and Jena (JEN) stations: ZAG, Croatia, epicentral distance De = 398 km, azimuth, az = 275°, incidence angle, ain = 44°, Wiechert seismographs, weight is 80 kg for horizontal components and 1300 kg for the vertical component, To = 4.3-5.1, Vo = 15-17; DBN, Nederland, De = 1366 km, az = 307°, ain = 0.0°, Galizin seismographs, To = 25 sec, Tg = 24 sec, Vo = 310); JEN, Germany, De = 918 km, az = 313°, ain = 0.0°, Wiechert seismograph, weight = 1200, 1300 and 15000 kg, To = 3.1-10.5 sec, Vo = 150-220. Oros [2011] digitized and corrected them to minimize the distortions and weak synchronicities between the components of the seismographs; e.g., the waveforms were aligned to the S wave arrival and the linear trend has been removed. The FMS was determined through the full waveform inversion in the frequency band 0.03-0.08 Hz using the ISOLA program [Sokos and Zahradnik, 2008]. The results are: centroid depth hc = 9.4 km, NP1 is 81°/52°/–23°, NP2 is 185°/72°/–140°, P-axis is 50°/41° and T-axis is 309°/120°, variance reduction is vr.32 = 24%, space variation of solutions, FMVAR = 16° ± 8°, seismic moment Mo = 3.24e16 (Mw = 4.96), the tensor torque with Double-Couple Component, DC = 91.2%, Compensated Linear Vector Dipole, CLVD = 8.8% and Isotropic Component, ISO = 0% (correlation corr = 0.52) (Figure 4a and b). The robustness of the solution was confirmed by the good fitting of the synthetic seismograms with the ones observed (Figure 4c) at Munich (MNH), Strasburg (STR) and Istanbul Kandilli (ISK) stations with unknown instrument characteristics. Moreover, the synthetic and observed wave spectra are comparable for the ZAG, DBN and JEN stations (Figure 4d), especially at frequencies where the amplification curves of instruments are maximum and constant ($f > f_0$; Wiechert seismographs) or where the maximum amplification variations are less than 5% (Galizin instrument). It is also evident the consistency of the N81°E nodal plane with the elongation of the maximum intensity isoseismal direction (Figure 4e) and STF fault orientation.

3.4 Focal mechanism uncertainties

Regardless of the methods used, the focal mechanisms are affected by inherent errors due to 1) data quality often altered by analysts (readings of the polarities, inadequate filtering, and wrong identified phases), 2) the seismic network configuration and 3) the used algorithms.

The HASH program computes many useful parameters for diagnosing the quality of solutions, such as:

1) the nodal plane errors (NPU, in degrees) as the root-mean-square angular difference between acceptable and preferred planes and that can be used statistically as 1σ (Hardebeck and Sherer, 2002). NPU is the best individual indicator of FMS quality, with all FMS with NPU ≤ 35° being rigorously determined and stable (quality A and B) [Kilb and Hardebeck, 2006],
2) the Station Distribution Ratio (STDR) that characterizes the relationship between the radiation pattern and the distribution of the data on the focal sphere regardless of their number (STDR = 0-1, low values meaning that most of the data are close to the nodal planes), being useful especially when the events are located at the edge of the station networks, grouped within a narrow azimuthal range and when only a few polarities are available and
3) the fraction of misfit polarities (F-Fit = 0-1, 0 means perfect fit) which shows whether the solutions are well constrained [Reasenberg and Oppenheimer, 1985].

We classified the solutions into four quality classes, denoted with letters A to D (A is the best quality) according to the NPU, STDR and F-Fit values [Hardebeck and Shearer, 2002]. When these parameters were contradictory, we used some parameters that can influence the FMS quality (Table 1). These have been determined from their relationship with NPU as suggested by Yang et al. [2012]; e.g. the number of polarities (No_Pol), the azimuthal gap of stations (Azp_gap), No of S/P ratios, take-off angle gap (Tko_gap), mean S/P ratio errors, magnitude and focal depth (Figure 5). Due to the large scattering of the data, we applied the local regression method Lowess type (Locally Weighted Scatterplot Smoothing), quadratic polynomial, with a smoother variable parameter between 0.25 and 0.5. It is clear that only between NPU and No_Pol and Azp_gap can be established deterministic relationships, as the elliptical density distributions and regression curves support (Figure 5a, b, c, d). The regression curves can be described by two linear components. One shows a direct link between the variables and the other is strongly affected by the smaller number of data and has no significant meaning for the analysis. The useful values for the quality diagnostic of the

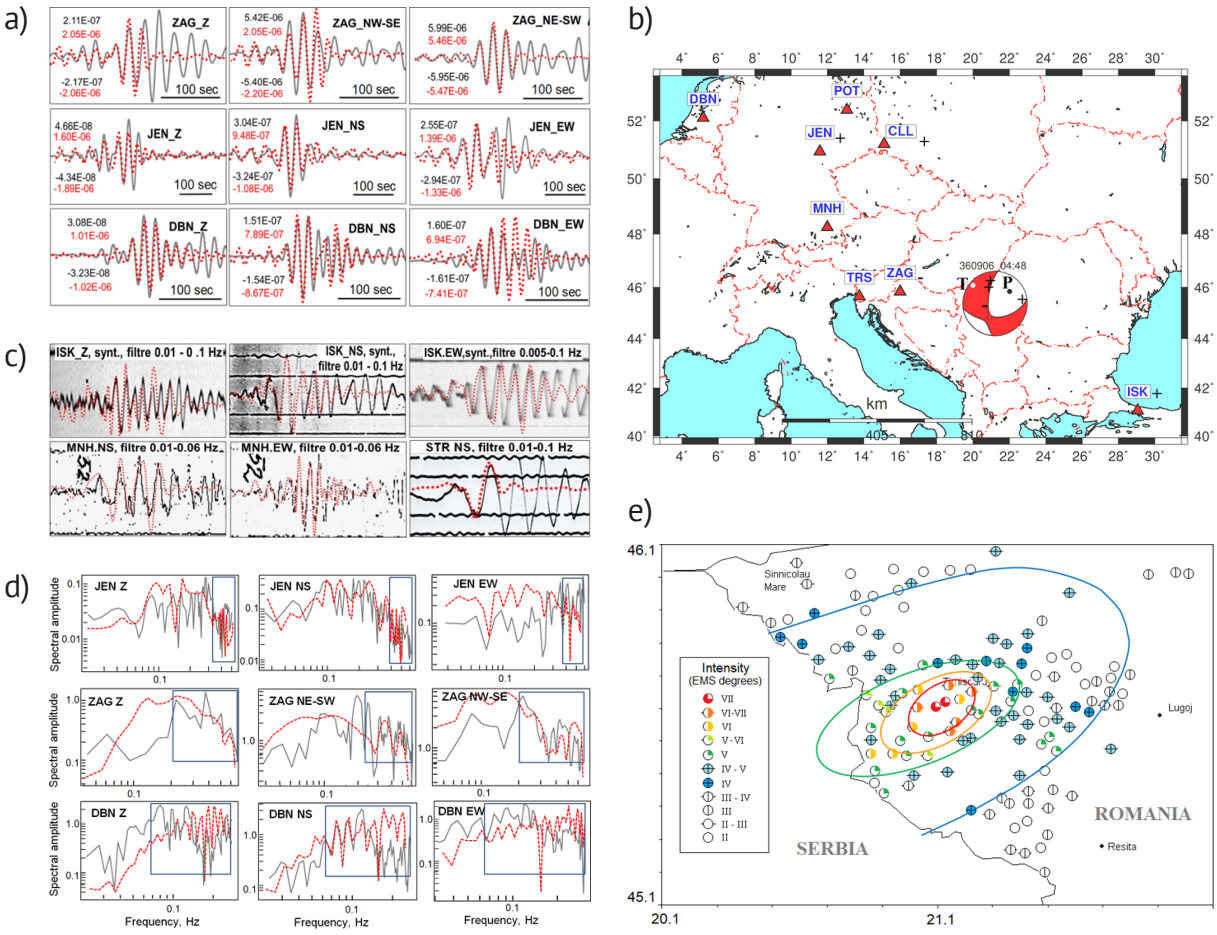

Figure 4. Focal mechanism solution computed for the Mw = 5.1, 06.09.1936 earthquake. The solution has been computed using the ISOLA program [Sokos and Zahradnik, 2008]. a) Comparison between observed (dark grey lines) and synthetic (dotted red lines) displacement waveforms computed for the HASH solution; ZAG, JEN and DBN are the analysed stations (maximum displacements are in meters). b) Distribution of the seismic stations used for inversion and analysis; P and T are kinematic axes, + and – are P polarities. c) Comparison between scanned analogue seismograms and synthetic waveforms computed for ISK (Istambul), MNH (Munich) and STR (Strasburg) stations; synthetic waveforms computed using Seisan program have been bandpass filtered with cut-off frequencies of 0.01 to 0.06 Hz and 0.005 to 0.1 Hz respectively. d) Uncorrected spectral amplitudes for synthetic (red dashed lines) and observed (black lines) seismograms at ZAG, JEN and DBN stations; the free period, fo of the Wiechert pendulums from JEN and ZAG stations that control the corner frequency of their response curve are presented; for Galizin instrument (DBN station) is noted the frequency range corresponding to maximum gain; the rectangles define the frequency ranges with constant (Wiechert seismographs) or very small variation (5%, Galizin seismometer) of the amplification of the instrument, respectively. e) Macroseismic map after Oros [2011].

FMS have been estimated from the regression curves and using a 70% density distribution. However, because the S/P ratios are very strong constraints in FMS estimation improving the final solutions, the Azp_gap and No_Pol lose or no longer have a significant weight on the final decision on the FMS stability. For this reason, the threshold values of these two quality parameters are different for the FMS determined only by polarity inversion (M1 mechanisms) and for those constrained by S/P ratios, or M2 mechanisms (Table 1).

Quality	NPU [°]	STDR	F-fit	Azp_gap [°]#	No_Pol#	No (%) of events
A	**≤ 25**	**≥ 0.5**	**≤ 0.15 (0.40^)**	≤ 65 (180^)	≥ 16 (6^)	675 (55.6)
B	**≤ 35**	**≥ 0.4**	**≤ 0.30 (0.50^)**	≤ 140	≥ 8 (4^)	315 (25.8)
C	**≤ 45**	**≥ 0.3**	**≤ 0.40 (0.50^)**	≤ 170	≥ 6 (4^)	142 (11.7)
D	**all other solutions with NPU ≤ 55°**; only for M1: Azp_gap ≥ 170°, No_Pol < 6					85 (6.9)

NPU is the average of the values estimated for the two nodal planes, M1 is the focal mechanism computed only by polarities inversion; ^ values for M2 solutions constrained with S/P ratios.

Table 1. Quality criteria after Hardebeck and Shearer [2002] with modifications.

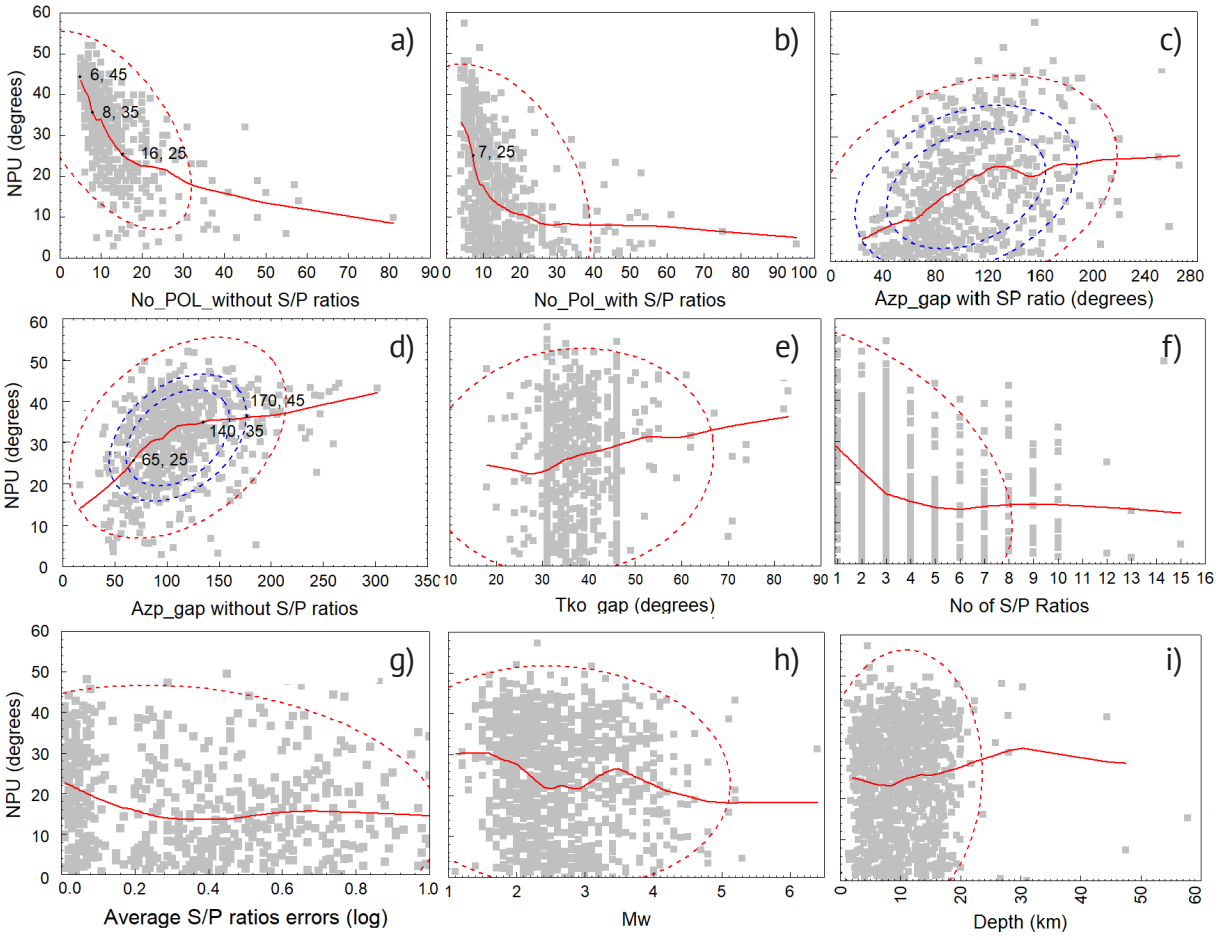

Figure 5. Nodal plane uncertainties (NPU) as a function of a) the number of polarities (No_pol) for mechanisms M1 and b) M2, c) azimuthal polarities gap (Azp_gap) for mechanisms M2 and d) M1, e) takeoff angle gap (Tko_gap), f) the number of S/P ratios, g) average S/P ratios errors, h) magnitude, i) depth. Thick red lines are regressions curves; dashed ellipses are 95% (red), 70% and 50% (blue) confidence and density data distribution.

Even if there is no deterministic relationship between NPU and STDR and F-fit, we used them as diagnostic parameters for FMS quality because by definition they may have decisive values for assessing the stability and reliability of the solutions. We also decided to use Tko_gap values because the density ellipse in Figure 5e shows A and B quality solutions (NPU < 35°) when Tko_gap < 70°.

The quality of FMS imported from literature was defined by taking into account the magnitude, the year in which each event occurred, the number of polarities, and epicentral distances.

3.5 Stress inversion of focal mechanisms

It is known that the focal mechanisms typology is controlled by the slipping on the faults and the P and T-axes do not correspond to the stress axes in a geological environment with pre-existing faults.

Thus, to understand the seismogenic features of the geological structures we need more data about the stress orientation and stress regime. To estimate the stress field parameters we applied the technique of formal inversion of the FMS. We used two free programs for comparative analysis and for validating the results, Zmap [Wiemer, 2001] and Win-Tensor [Delvaux and Sperner, 2003], respectively. Both of them compute the main stress axes of the reduced stress tensor (S1, S2, S3 by Zmap, σ1, σ2, σ3 by Win-Tensor, S1/σ1 > S2/σ2 > S3/σ3) and the stress ratio R = S2-S3/S1-S3 for each selected dataset. They also quantify the heterogeneity of the stress field through the misfit angle; e.g. β computed using Zmap as a cumulative misfit of a set of focal mechanisms to a given stress tensor, and α computed using Win-Tensor as average angular misfit deviation between observed and modelled slip directions. Zmap applies Michael's linearized inversion method [Michael, 1984, 1987; Michael et al., 1990], a bootstrap approach to assessing inversion uncertainty and Zoback's criteria to define the stress regime [Zoback, 1992]. It also displays in 2D space the stress field heterogeneity (variance, V in %). Thus, the stress field is homogeneous and one stress tensor can explain the focal mechanisms if V < 0.2. The higher values of V, meaning spatially or temporally heterogeneous stress field within the analysed volume, suggest a poor fit to one stress tensor and large variability in focal mechanisms [Wiemer, 2001 and references therein]. The program creates useful maps to assess the spatial resolution of the data and to investigate the 3D variations of the stress field (homogeneity, stress direction, faulting style). Win-Tensor uses an improved Right Diedron method of Angelier and Mechler [1977]. The fault (NP1) and auxiliary (NP2) planes of the FMS are discriminated against each other - based on the mechanical compatibility with the calculated stress tensor criteria. The programme also computes the slip-tendency (ST), representative FMS for particular stress conditions, horizontal stresses (SHmax and Shmin) and a stress regime index, R′ (R′ = 0-3). The ST, as a probability of reactivation of geological structures, is defined by the shear-to-normal stress ratio that has to exceed the friction coefficient on the fault surface. R′ index expresses numerically the stress regime as follows: R′ = R when σ1 is vertical (extensive), R′ = 2-R when σ2 is vertical (strike-slip) and R′ = 2 + R when σ3 is vertical (compressive) where R is the stress ratio [Delvaux and Sperner, 2003; Delvaux et al., 1997].

We used all data in inversion to avoid alteration of the primary datasets by eliminating mechanisms even totally incompatible with final solutions as recommended by Delvaux and Barth [2010] and knowing that the inversion is reliable when a wide variety of mechanisms is used [Delvaux and Sperner, 2003].

4. Results and discussion

4.1 Focal mechanisms solutions and active tectonics

The new catalogue is presented in the Appendix (Table 3). It contains FMS computed for 1217 earthquakes recorded between 1901 and 2018. The frequency of the most stable and reliable mechanisms (quality A and B) is over 80% (N = 990). The contribution of the M2-type mechanisms is substantial (N = 719 or 59.1%), these having the quality A, B, C and D in proportion of 73.0%, 19.2%, 6.5% and 1.3%, respectively (Figure 6). The contribution of M1-type mechanisms accounted for 37.4 % (N = 456) of all inputs in the catalogue with 62% quality solutions A and B, 20% quality C and 12% quality D. The high quality of the solutions is reflected in the values of STDR > 0.5 (61%, M1; 66% M2), No_Pol > 8 (69%, M1; 79%, M2), No_S/P ratios > 3 for 66% of mechanisms, F-fit < 0.3 (90%, M1; 89%, M2) (Figure 6a-e). The Az_gap is on average 106° ± 42° suggesting a good station coverage. High levels of Az_gap are common at the edges of the region, at the borders with neighbouring countries.

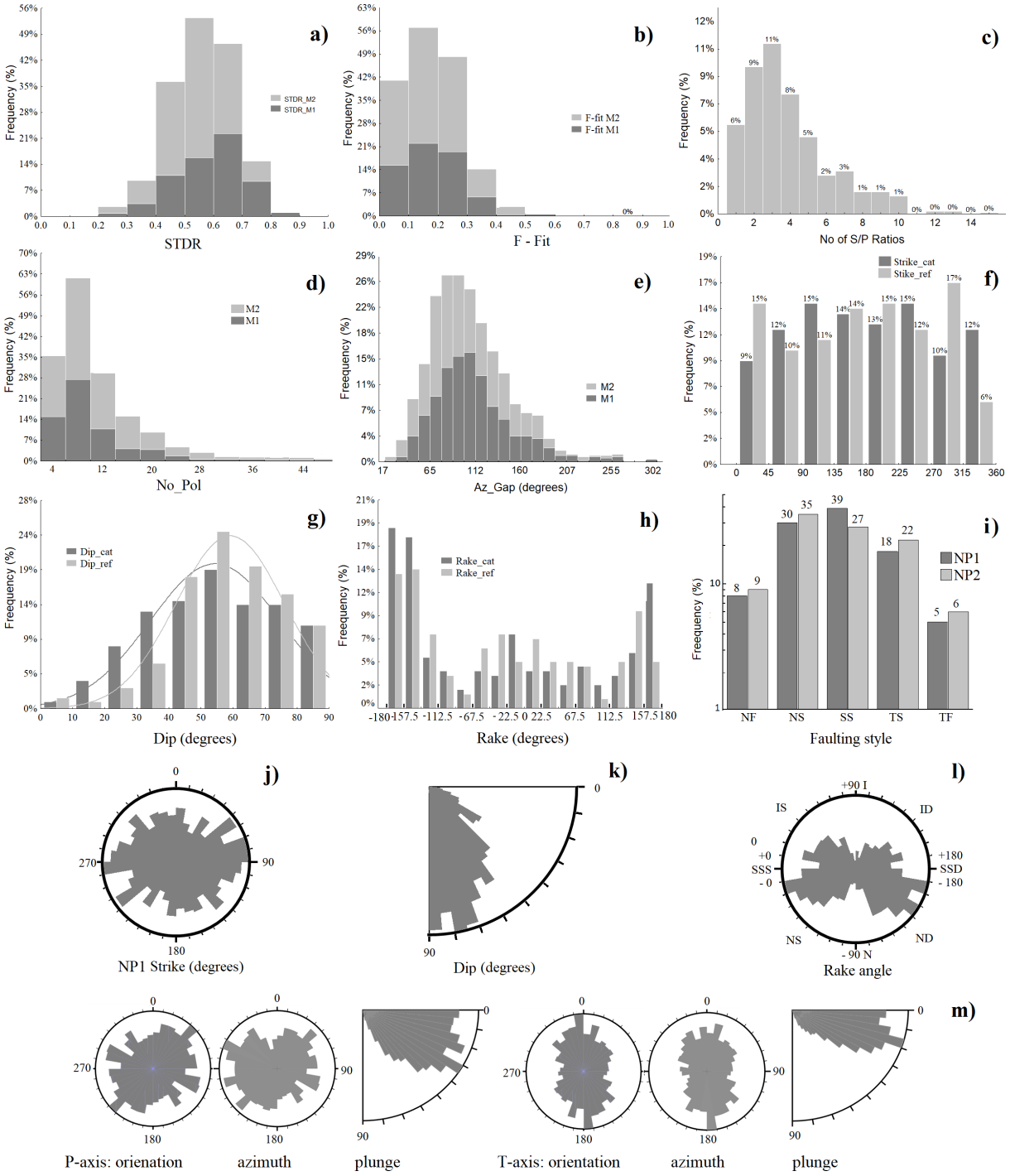

Figure 6. Histograms of the (a) STDR, (b) F-fit, (c) No_SP ratios, (d) No_Pol, (e) Az_gap computed for the M1 (N = 455) and M2 (N = 719) mechanisms, respectively. (f) Distribution of the strike, (g) dip and (h) rake of the NP1 plan for 175 imported (#ref) and recomputed (#cat) mechanisms; normal fitting curves are shown for the dip parameter. Estimated faulting style on the rake angle basis [Aki and Richard, 1980]; NP1 and NP2 are the nodal planes (i). Polar diagrams for NP1: strike (j), dip (k), and rake angle/faulting style: SSD/S = right/left-lateral strike-slip, N = normal, ND/S = oblique dextral/sinistral normal, I = reverse, ID/S = oblique dextral/sinistral reverse (l). Polar diagrams for P-, T-axis orientation, azimuth and plunge (bin size 10°) for the whole study region (m).

We imported from the literature 218 mechanisms, 210 appreciated with quality B (solutions estimated using only polarities, N > 10) and with 8 quality A (mechanisms determined through the moment tensor inversion technique by international agencies, such as ISC and HRVD). Only 43 of the imported solutions could not be revised due to a lack of primary data sources (seismograms, bulletins). By reviewing, we obtained N = 175 very different solutions

(Figure 6f-h) showing different parameters from the original imported ones. On average, the difference between the strikes of the NP1 planes is 24° ± 17°, but there is no predominant direction for either new or imported solutions (Figure 6f). Most new solutions have NP1 nodal plane with angles < 40° and very different rake angle values so that a sensitive change in the faulting style compared to that inferred from imported solutions can be noted, i.e. the right transtensive (rake –112.5° to –157.5°) and right strike-slip (rake –157.5° to 157.5°) faulting becomes predominant compared to the left transtensive and transpresive (rake ± 22.5° to ± 67.5°) and right transpresive ones (rake 22.5° to 67.5° and 112.5° to 157.5°) (Figure 6h).

A first-order analysis of FMS provides useful information for the assessment of the present-day deformation and for doing a study compared to results obtained by other authors with other data sets. It is based on statistical distributions of the fault planes' strike and dip, rake angle and the azimuth and plunge of the P and T axes (Figures 6 and 7). Previous studies of FMS carried out at the crustal level in Romania have generally used small samples and the results were often preliminary, contradictory and inconclusive [e.g. Bala et al. 2003; 2019; Radulian et al., 1996; 2000; 2002; 2018]. Radulian et al. [1996] used, for example, 57 FMS and described the crustal stress field in Romania by 1) EW compression all along with the eastern border of the Pannonian Depression and in the North of Eastern Carpathians, 2) NW-SE compression in the South-West Carpathians Bend area and 3) EW-oriented extension in the Southern Carpathians. On the contrary, Oros [2011] used 140 FMS published by Oros et al. [2008] and showed that the southeastern border of the Pannonian Depression (BA zone) is characterized by NE-SW oriented compression and the western edge of the South Carpathians (DA zone) is characterized by an extensive tectonic regime with normal faulting on NNE-SSW and NE-SW structures (e.g. WF, CJF). Radulian et al. [2000] analyzed 8 FMS in the FC zone and Bala et al. [2003; 2019] combined data in FC and CSC zones (N = 17), both studies concluded that the tectonic regime is extensive but the fault planes are randomly oriented and a clear stress regime cannot be defined. Radulian et al. [2018] showed, however, that reverse faulting on ENE-WSW orientated planes (N = 18 FMS) is dominant on the orogen-Moesian Platform contact zone.

Our statistics of the FMS parameters highlight, first of all, a high diversity of mechanisms which means high-quality datasets for reliable stress inversion at regional or local scales and also reflects the complex active tectonics and local variation of the faults reactivation conditions, such as dominant local stress sources and some geological conditions that modify the frictional resistance on fault planes (e.g. fluids under pressure, rupture permeability, weak materials). We evaluated the faulting style using the criterion of Aki and Richard [1980] which is based on rake angle and realistically classifies the mechanisms knowing that earthquakes are manifested by displacements on the faults, here expressed by slipping vectors. Although this criterion may be affected by the duplicity of the nodal planes, we will use in the analysis only the values obtained for the fault plane (nodal plane NP1) because the differences between the two nodal planes are insignificant (Figure 6i).

The histogram in Figure 6i shows that the strike-slip and normal strike-slip faultings are dominant in the study region, but there have also been a significant number of inverse strike-slip faults. The polar diagrams in Figure 6j-6m highlight regional active tectonics with structures generally oriented EW and ENE-WSW that have been reactivated mainly as sinistral and dextral strike-slip (rake: –10 to –20° and –160 to –170°) and dextral normal-strike-slip faults (rake: –140 to –150°), most of them high-angle (dip > 70°) or vertical. These faults are very well correlated with the fault systems that controlled the kinematics and neotectonic evolution of the region; e.g. NTF, STF, SCF, CJF (see Figure 1; [Linzer et al., 1998; Polonic, 1985; Sandulescu, 1984 and references therein]). The P- and T-axis geometry (Figure 6m) support this faulting style; e.g. the T-axis (plunge: 10-20°, azimuth N170-180°) is almost perpendicular to the main reactivated structures and the P-axis (plunge < 40°, oriented NE-SW) defines a near-optimal reactivation angle of 30°-40° to these pre-existing structures [Celerier, 2008; Fossen, 2010]. However, the multimodal distribution of P-axis azimuth (N220-230°; N260-270°; N290° and N40-50°) suggests a complex interference of the first-order stress with stronger local sources such as elevated topography, crustal and lithospheric inhomogeneities, thermal stress and stress reorientation at fault tips and active major faults as other authors estimated [e.g. Bada et al., 1998 and references therein; Muller et al., 2010]. To detail these statistics, we divided the region into three large sectors individualized on the morpho-structural and tectonic features basis. As can be seen in Figure 7, each of the three sectors displays particular patterns of the active faults orientation, faulting style and P and T axes geometry.

The western sector (BA, BZ and the western half of CM), where like-graben neotectonic structures of Pannonian Depression develop, is characterized by most left and right strike-slip with large normal components faults (rake: 15 to 30° and –157 to –165°) oriented EW and ENE-WSW. The P-axis is oriented towards SW (azimuth N220-230°) in the direction of the Africa-Europe collision area. This pattern is different from that developed by Radulian et al. [1996; 2002] and shows similarities with the post-Paleogene deformations described by Linzer et al. [1998].

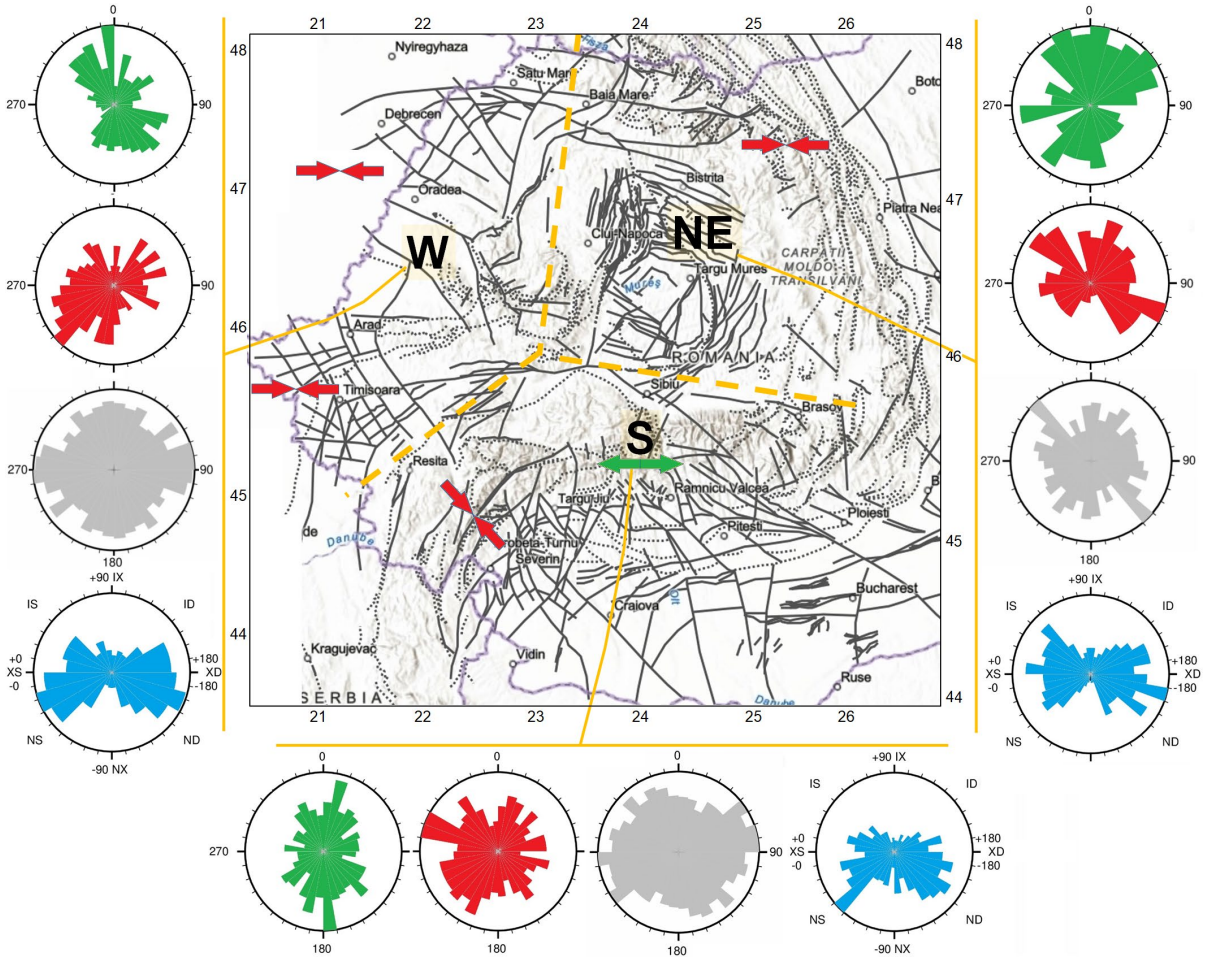

Figure 7. Polar diagrams of P- (red), T-axis (green) azimuth, strike (grey) and rake (blue) of NP1 and NP2 computed for the western (W), north-eastern (NE) and southern (S) morpho-structural units in the region. Red and green arrows are the P and T axes directions after Radulian et al. [1996].

Another sector (northeastern sector) overlaps the depressions, basement nappes, ophiolitic crustal blocks and volcanic structures which characterize the crustal geology of the Transylvania Basin and the border of the Eastern Carpathians (CM-eastern half, TR and EC zones). The earthquakes occurred mainly on right strike-slip faults (rake: −170°) and secondary on thrust/normal strike-slip faults (rake −40° and 50°) mainly oriented NW-SE, parallel to Carpathians structures. The azimuth of the P-axis is N110° towards the compression source in the South-East Carpathians Bend area [e.g. Polonic et al., 2005]. The T-axis azimuth varies in very large limits, from parallel to perpendicular on local structures, but on average it is consistent with the NS regional trend.

The third or Southern sector overlaps South Carpathians (DA, CSC, FC zones) and is characterized by EW to ENE-WSW oriented structures that have been reactivated as left normal strike-slip faults (rake: −40 to −50°). We note the insignificant number of reverse faults as Radulian et al. [2018] observed, too. Worth mentioning the T-axis is oriented towards North and South (azimuth N170-180° and N10-20°), perpendicular to the extension direction calculated by Radulian et al. [1996] and that estimated by Linzer et al. [1998] for the Quaternary period through microtectonic studies. P-axis is oriented towards WNW (azimuth N290°) and correlates with the direction estimated in the south-western part of South Carpathians by Radulian et al. [1996], Oros [2011], Placinta et al. [2016] and Popa et al. [2018].

4.2 Stress field and seismogenic potential of the geological structures

We performed the formal inversion of the focal mechanisms using high-quality datasets (Nmin = 8 FMS) selected for the known seismogenic zones and smaller areas defined by clusters and particular tectonics. The results are presented in Table 2 and Figures 8-14.

Zone/sub-zone	N FMS	σ1 [°]	σ2 [°]	σ3 [°]	R	R′	α [°]	S_{Hmax} [°]	S_{hmin} [°]	TSR*
Intracarpathian region (RICR)	990	296/70 ± 51.2	80/17 ± 54.6	173/11 ± 25.7	0.79	0.79 ± 0.42	75 ± 54	86 ± 21	174	SSE
Western Sector	296	247/35 ± 31	72/55 ± 52	338/2 ± 47	32	1.68 ± 0.18	70 ± 51	68 ± 32	158	PSS
North-eastern Sector	164	276/12 ± 16.8	58/75 ± 44	184/9 ± 43	0.02	2.02 ± 0.26	72 ± 54	96 ± 13.5	6	SSC
Southern Sector	458	244/68 ± 29.3	91/20 ± 55.8	358/9 ± 50.5	0.19 0.15±	0.19 ± 0.16	72 ± 45	79 ± 52	169	REx
Crisana-Maramures (CM)	67	104/2 ± 11.8	198/66 ± 50	13/24 ± 53	0.03	1.97 ± 0.39	62 ± 52	103 ± 12	13	CSS
1. Sighet	21	122/18 ± 10.5	218/16 ± 13.8	347/65 ± 13.0	0.11	2.11 ± 0.16	49 ± 53	121 ± 9	31	SSC
2. Baia Mare	12	111/19 ± 15.0	213/30 ± 22.8	355/53 ± 20.9	0.44	2.44 ± 0.23	36 ± 42	105 ± 14	15	PC
3. Satu Mare	8	276/12 ± 7.9	169/54 ± 18.9	14/33 ± 17.8	0.40	1.60 ± 0.24	57 ± 56	99 ± 5	9	PSS
4. Crisana	8	316/59 ± 7.6	56/6 ± 19.5	149/30 ± 18.2	0.32	0.32 ± 0.15	42 ± 36	82 ± 37	172	PEx
5. Transcarpathian Basin	10	255/65 ± 29.7	90/24 ± 29.7	358/6 ± 9.3	0.97	0.97 ± 6.7	36 ± 22	88 ± 6.7	178	SSE
Banat (BA)	212	240/19 ± 45.1	77/70 ± 44.4	332/5 ± 21.3	0.85	1.15 ± 0.49	68 ± 60	62 ± 21	152	ESS
1. Banloc	19	36/19 ± 18.1	163/60 ± 25.8	298/22 ± 19.6	0.17	1.83 ± 0.28	56 ± 54	35 ± 7	125	CSS
2. Voiteg-Liebling	112	281/62 ± 53.0	66/24 ± 53.1	163/14 ± 8.5	0.99	0.99 ± 0.31	66 ± 53	73 ± 8	163	SSE
3. Timisoara	17	39/45 ± 4.4	251/40 ± 44.1	146/16 ± 44.2	0.01	0.01 ± 0.03	46 ± 37	39 ± 5	129	REx
4. Buzias-Mosnita	14	260/28 ± 13.7	130/51 ± 30.1	5/25 ± 14.5	0.25	0.75 ± 0.26	60 ± 59	84 ± 15	174	PEx
5. Lucaret-Masloc	24	300/55 ± 10.8	65/22 ± 13.3	166/26 ± 11.2	0.31	0.31 ± 0.15	38 ± 28	97 ± 17	7	PEx
6. Vinga-Varias-Biled	14	57/18 ± 12.8	195/67 ± 19.4	322/14 ± 18.9	0.26	1.74 ± 0.2	47 ± 58	56 ± 9	146	CSS
7. Teremia	12	242/19 ± 11.7	39/69 ± 14.0	149/8 ± 7.9	0.17	1.83 ± 0.16	31 ± 35	62 ± 2	152	CSS
8. Sinnicolau Mare	8	270/17 ± 5.0	3/9 ± 33.3	119/71 ± 33.6	0.09	2.09 ± 0.08	36 ± 38	90 ± 3	0	SSC
Bekes-Zarand (BZ)	38	215/15 ± 15.7	23/75 ± 50	124/3 ± 49	0.06	1.94 ± 0.18	60 ± 50	35 ± 12	124	CSS
Danube (DA)	139	328/74 ± 19.7	103/12 ± 52.4	196/11 ± 49.0	0.09	0.09 ± 0.13	62 ± 44	124 ± 47	34	REx
1. Sichevita	18	322/74 ± 3.1	146/16 ± 33.0	55/1 ± 33.1	0.02	0.02 ± 0.04	49 ± 37	143 ± 20		REx

Zone/sub-zone	N FMS	σ1 [°]	σ2 [°]	σ3 [°]	R	R′	α [°]	S_{Hmax} [°]	S_{hmin} [°]	TSR*
2. Mehadia-Herculane	49	285/69 ± 9.7	181/5 ± 26.8	89/20 ± 26.4	0.08	0.08 ± 0.07	57 ± 42	121 ± 39	31	REx
3. Plugova-Godeanu	24	28/81 ± 32.4	275/3 ± 32.7	184/8 ± 11.9	0.80	0.80 ± 0.22	59 ± 42	94 ± 10	4	SSE
4. Moldova Noua	14	302/51 ± 5.6	100/37 ± 15.0	199/11 ± 15.4	0.18	0.18 ± 0.09	4 ± 5	117 ± 8	27	REx
5. Moldova Noua-Serbia	20	102/44 ± 28.4	273/45 ± 28.4	7/5 ± 5.9	0.94	1.06 ± 0.09	44 ± 45	97 ± 4	7	ESS
6. Serbia-Sud	13	104/23 ± 4.2	204/21 ± 26.8	332/58 ± 26.9	0.02	2.02 ± 0.07	53.3 ± 45	104 ± 3	14	SSC
7. Serbia-West	12	278/21 ± 10.4	180/19 ± 33.1	50/61 ± 34.3	0.13	2.13 ± 0.11	49 ± 49	99 ± 8	9	SSC
Fagaras-Campulung (FC)	127	243/56 ± 27.9	71/34 ± 40	339/4 ± 36.4	0.20	0.2 ± 0.18	71 ± 51	66 ± 34	156	REx
1. Olt Valley	43	204/50 ± 31.9	38/39 ± 32.4	302/7 ± 10.2	0.86	0.87 ± 0.26	56 ± 44	32 ± 7	122	SSE
2. Fagaras-Iezer	20	243/31 ± 26.5	70/59 ± 26.5	337/2 ± 3.8	0.96	1.04 ± 0.04	32 ± 38	66 ± 3	156	ESS
3. Campulung	14	110/22 ± 20.4	262/65 ± 24.7	16/11 ± 14.8	0.33	1.67 ± 0.18	45 ± 33	108 ± 5	18	PSS
4. Comarnic-Tirgoviste	17	160/12 ± 22.2	18/75 ± 26.5	253/9 ± 23.1	0.41	1.59 ± 0.35	72 ± 55	161 ± 14	71	PSS
Transylvania (TR)	13	40/12 ± 53	170/72 ± 49	307/13 ± 16	0.73	1.27 ± 0.27	62 ± 60	37 ± 9	127	ESS
Eastern Carpathians (EC)	49	317/4 ± 22.1	226/18 ± 22.7	59/72 ± 23.2	0.29	2.29 ± 0.24	69 ± 4	138 ± 22	48	PC
Central-South Carpathians (CSC)	144	288/42 ± 25.3	84/44 ± 33.2	186/12 ± 28.9	0.37	0.37 ± 0.23	65 ± 48	101 ± 21	11	ESS
1. Hateg Basin	86	308/65 ± 53	93/21 ± 53.2	188/13 ± 9.1	0.99	0.99 ± 0.20	38 ± 38	98 ± 7	9	ESS
2. Godeanu Mts	21	254/75 ± 36.1	78/15 ± 36.4	348/1 ± 8.8	0.45	0.45 ± 0.29	49 ± 42	78 ± 9	168	PEx
3. Petrosani-Closani	36	279/58 17.9	92/31 ± 33.3	184/3 ± 29.2	0.15	0.15 ± 0.13	55 ± 42	97 ± 19	7	REx
4. Tirgu Jiu	18	33/4 ± 14	295/65 ± 58.8	125/25 ± 58.1	0.09	2.22 ± 0.23	53 ± 55	33 ± 3	123	CSS

*Tectonic stress regime defined after Devaux et al [1997]: REx = radial extensive (R′ = 0-0.25, σ1 vertical), PEx = pure extensive (R′ = 0.25-0.75, σ1 vertical), ESS = transtensive or extensive strike-slip (R′ = 0.75-1.0, σ1 vertical), SSE = transtensive or strike-slip extensive, (R′ = 1.0-1.25, σ2 vertical), PSS = pure strike-slip (R′ = 1.25-1.75, σ2 vertical), SSC = transpressive or strike-slip compressive (R′ = 1.75-2.0, σ2 vertical), CSS = transpressive or compressive strike-slip (R′ = 2.0-2.25, σ3 vertical), PC-pure compressive (R′ = 2.25-2.75, σ3 vertical), RC = Radial compressive (R′ = 2.75-3.0, σ3 vertical)

Table 2. Results of the stress tensor inversion using the Win-Tensor program [Delvaux and Sperner, 2003]. S_i (σ_i) = stress axes, R = stress ratio, R′ = stress regime index, α = misfit angle, TSR = tectonic stress regime

The independent evaluation of our results is difficult because there are very few papers published until now that investigated the present-day crustal tectonic stress and deformation in the study region using techniques of FMS inversion. Thus, Bada et al. [2007] and Oros [2011] applied the inversion technique developed by Delvaux and Sperner [2003] in the southeastern corner of the Pannonian Depression. The first authors found strike-slip kinematics and the others an oblique normal strike-slip one, while the maximum horizontal stress, SHmax is oriented NE-SW in both studies. Several studies used alongside focal mechanisms and other stress indicators (geological and borehole data) to determine the horizontal stress tensor and to compute a smoothed stress field; e.g. Muller et al. [2010] show that the eastern half of Romania can be characterized by a short wave-length stress pattern with small patches of different stress orientation controlled by local stress sources. Heidbach et al. [2018] used a fixed search radius of 500 km on a global two degrees grid and compute a smoothed stress map (first-order stress map) with the SHmax-oriented NNE-SSW in the West of Romania and NE-SW in the East. The stress orientation estimated in Transylvania Depression by Zugravescu et al. [2005] and Zugravescu and Negoita [2010] using borehole data can be described by NE-SW-oriented SHmax in the West and South-West and NNW-SSE at the contact with the Eastern Carpathians. However, results based on geological data have to be used with great caution as they could not represent the contemporary crustal stress pattern [Muller et al., 2010].

First of all, we can conclude that our data provides rigorous scientific support to investigate the stress-strain states with a very good spatial resolution at different scales, as the maps from Figure 8 (left) show; e.g. the datasets with $N > 8$ FMS allow mapping stress inversion results both at the level of tectonic blocks and the small structures/faults level, of a few kilometres (Figure 8a). These maps have been constructed using Zmap software, a grid with spaced nodes at 0.1° and constant samples with $N = 8$, 15, 30 and 50 FMS near each node. It can be observed that the heterogeneity o the stress field (variance), S1-axis orientation and stress regime vary with the increase/decrease in the number of FMS used in the inversion. Thus, for example, a heterogeneous stress field with $V < 0.3$, EW-oriented S1-axis and a strike-slip stress regime characterize the CM zone if $N = 50$ FMS (resolution 50-70 km) (Figure 8d). The model gradually changes on a local scale when $N = 15$-30 FMS and spatial resolution is 15-50 km (Figure 8 b and c): 1) the S1-axis rotates to NE-SW in the South-West, EW in the centre and NW-SE in the East, 2) the stress regime became extensive (normal faults) in the South-West and North-West where the Neogene basinal structures of Pannonian Basin develop and compressive (thrust faults) in the East and North-East within areas of the Carpathian nappes, 3) the homogeneity increases and reaches different values in the structures of the orogen and those of the Pannonian Basin. If $N = 8$ FMS (resolution up to 5 km and lower) the WNW-ESE direction of the S1 axis in the western half of the zone (along with the NTF system) and the NW-SE in the East (along the thrust faults of nappes structures) become predominant (Figure 8a, middle). The stress regime remains extensive and strike-slip in the West and compressive in the East, while the homogeneity increases significantly ($V < 0.25$) within the Carpathians structures.

The stress field model in Figure 8 shows three large areas that generally fit very well with the three morpho-structural sectors defined above ($N = 50$ FMS, Figure 8d). It also displays sharp changes, over very short distances (up to 5 km) of S1-axis orientation and faulting style from one seismogenic zone to another and on or near the active major faults. Muller et al. [2010] explain these kinds of shorth-scale variability of SH orientations in the eastern half of Romania by local sources whose magnitudes are comparable to or even higher than the regional differential stress magnitudes. Comparing our model in Figure 8d ($N = 50$ FMS and resolution 50-70) with the first-order stress computed by Heidbach et al. [2018] we can note that S1-axis rotates from NE-SW to EW and NW-SE from the western to northern and eastern areas following the P-axis trend in Figure 7. The Southern Carpathians exhibit a sinusoidal pattern of S1-axis orientation under an extensive stress regime (normal and normal-strike slip faultings). S1-axis rotates over distances of several tens km from NE-SW to EW and then NW-SE in the two main zones, DA and FC. A similar model of the S1 axis rotation can be described for the BA zone, but the tectonic regime is mainly strike-slip. S1-axis rotates from NW-SE to EW and NE-SW in the CSC zone but the stress regime is strike-slip and compressive at the contact between orogen and Moesian Platform as Radulian et al. [2018] observed in the South of the FC zone.

The kinematics of faulting is also changing between the three morfo-structural sectors, from strike-slip in the West to normal in the South and thrust in the East. These changes are obvious even locally in or between the seismogenic zones when fewer mechanisms were used in inversion (Figures 8a and b). It is worth noting the orthogonality of the S1-axis in the contact areas between the Southern Carpathians, Pannonian Basin and Eastern Carpathians, which would suggest a strong influence of the 2nd and 3rd-order stress field, e.g. ongoing activity and structural and rheological details of the fault systems, a large area with magmatic intrusions along with WF [Sandulescu, 1984], high contrasts in topography, contrasting recent vertical movements and lithosphere inflexion in the West [Zugravescu and Polonic, 1997; Polonic, 2005] and NW-oriented compression in South-East [Polonic et al., 2005; Zugravescu et al., 2005; 2010; Muller et al., 2010].

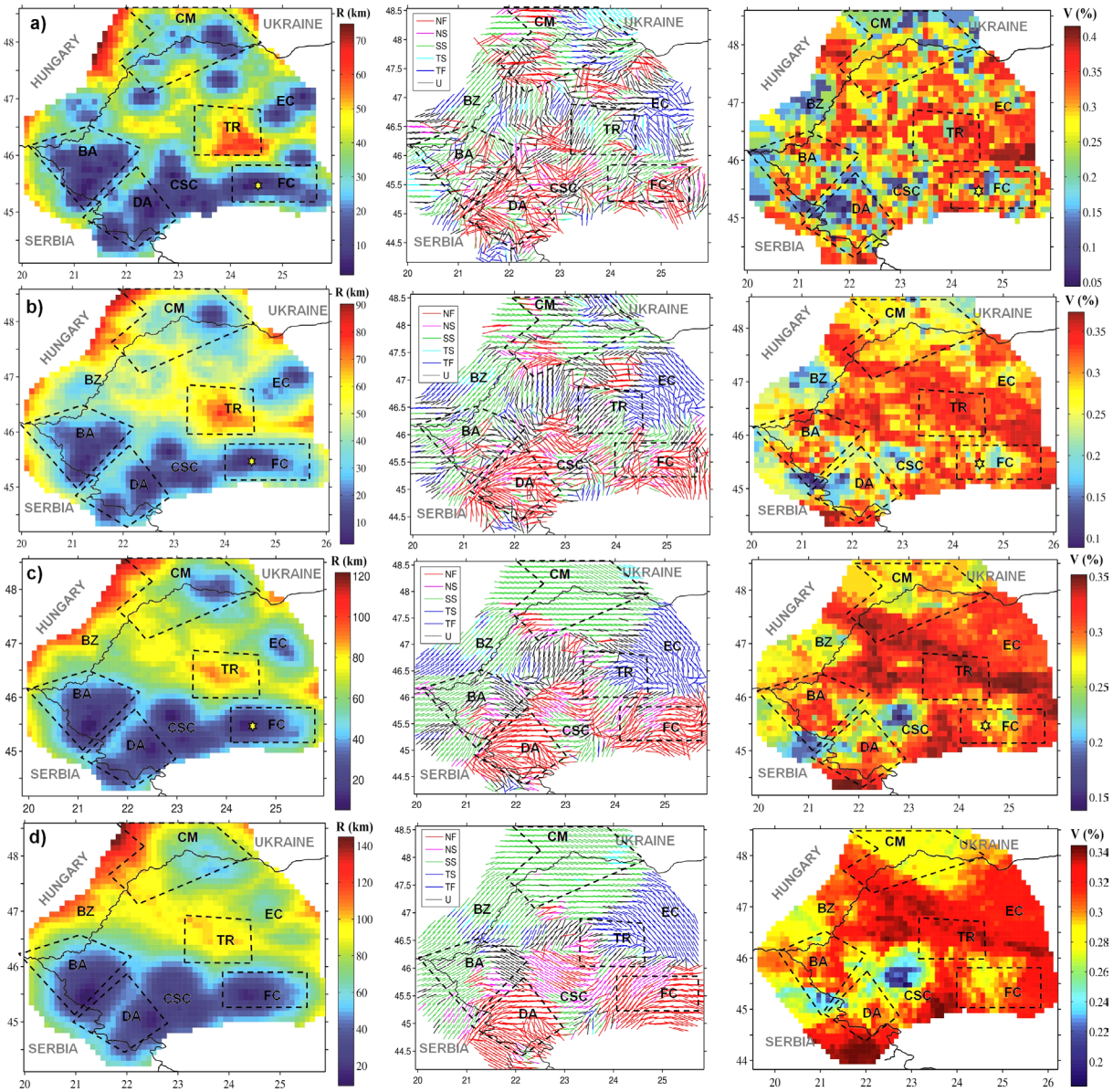

Figure 8. Stress tensor inversion results obtained using the Zmap program [Wiemer, 2001] and a grid-scale of 0.1x0.1 degrees, N = 8 events per grid node (a), N = 15 events per grid node (b), N = 30 events per grid node (c) and N = 50 events per grid node (d). The spatial resolution, R (km) (left panels), the orientation of S1 and faulting style (middle panels) and the variance V of the stress tensor at each node (right panels) are presented for each dataset. Dashed black polygons are the known seismogenic zones in the region (see Figure 1 for details).

Given the short wave-length stress patterns highlighted above and the geological and structural complexity of the region, we performed the inversion of stress tensor using datasets defined at seismogenic zones scale and several smaller data subsets (Nmin > 8 FMS) defined on a tectonic and seismicity basis (clusters) within each seismogenic zone (Table 2 and Figures 9 to 14) to identify localized stress changes and understand their impact on the seismotectonic features for seismic hazard studies.

4.2.1 Crisana-Maramures seismogenic zone (CM)

The stress tensor inversion in the CM zone has been performed based on N = 67 FMS (Figure 10). The results describe a heterogeneous contemporary stress field ($\alpha = 62° \pm 52°$), characterized by a transpressive stress regime with SHmax-oriented WNW-ESE. Concerning the first-order stress computed by Heidbach et al. [2018]

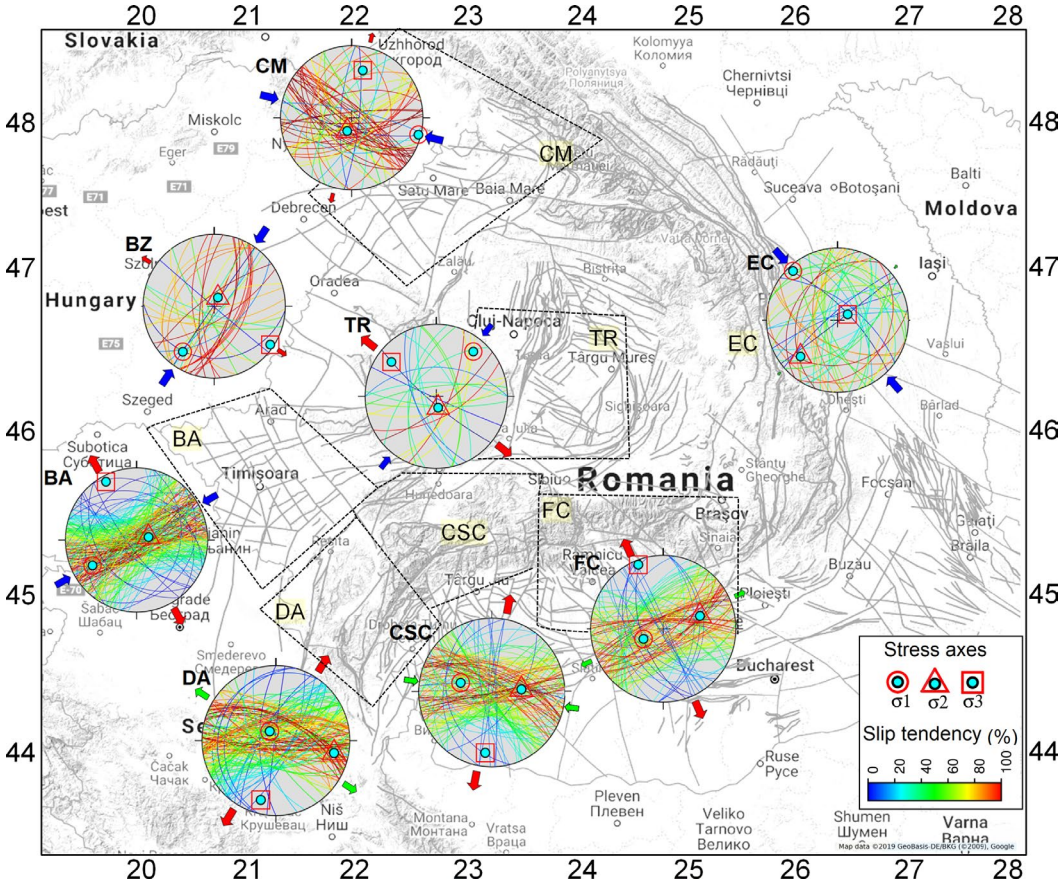

Figure 9. Stress inversion results computed for the main seismogenic zones using the Win-Tensor program (Wulff lower hemisphere projections); the NP1 nodal planes (cyclographic traces) and their Slip Tendency are displayed on the colour scale. The arrows are the 3 principal stress axes and related SHmax and Shmin (arrows outside of the stereograms). Their length and colour symbolise the horizontal deviatoric stress magnitude relative to the isotropic stress (σi) and are in function of stress regime and stress ratio: blue inward arrows are always SHmax (σ1 is subhorizontal), red outward arrows are always Shmin (σ3 is subhorizontal), green arrows are σ2 stress axes (outward when extensional (σ2 < σi) or inward when compressional (σ2 > σi)).

the SHmax is rotated clockwise about 90°, but it is parallel to the SHmax estimated by Bada et al. [1998; 2007] and the compression determined by Radulian et al. [1996]. SHmax is parallel to the EW-oriented neotectonic active fault systems (NTF system and faults bordering like-graben structures and depressions) and to the most common Carpathian structures (basement nappes) whose ongoing activity and structural geometry together with topography and fluid under pressure could be analyzed as the main local stress sources (the 3rd order stress field) that cause the drastic rotation of SHmax. The high-angle or vertical structures oriented NW-SE, NE-SW to EW and NS-oriented low-angle faults can be reactivated under these stress conditions as strike-slip and thrust faults, respectively (ST > 80%).

To detail the 3rd-order stress field sources imagine we proceeded to an inversion based on 5 smaller datasets (Nmin = 8 FMS) that represent clusters located within structures with different neotectonic history (Figure 10); e.g. extensional structures (grabens and depressions) belonging to the Pannonian Basin in the West (clusters no. 3, 4, 5) and the basement nappes and Neogene volcanic bodies of the Carpathians in East (clusters no. 1 and 2) [Polonic, 2005; Sandulescu, 1984]. SHmax has comparable orientations in the 5 clusters, the individual differences from the average value (N103°) being smaller than its standard deviation (± 12°). The stress regime that changes suddenly over short distances highlights notable differences between clusters. In the West, a pure-extensive (cluster 4) to transtensive (cluster 5) tectonic regime characterizes the areas with neotectonic basinal structures and where significant negative vertical recent movements are recorded [e.g. Polonic, 2005; Zugravescu and Polonic, 1997]. It is changing to a strike-slip (cluster 3) then transpressive and pure compressive regime (clusters 1 and 2) at the depression-orogen contact and in the Carpathians basement nappes, respectively.

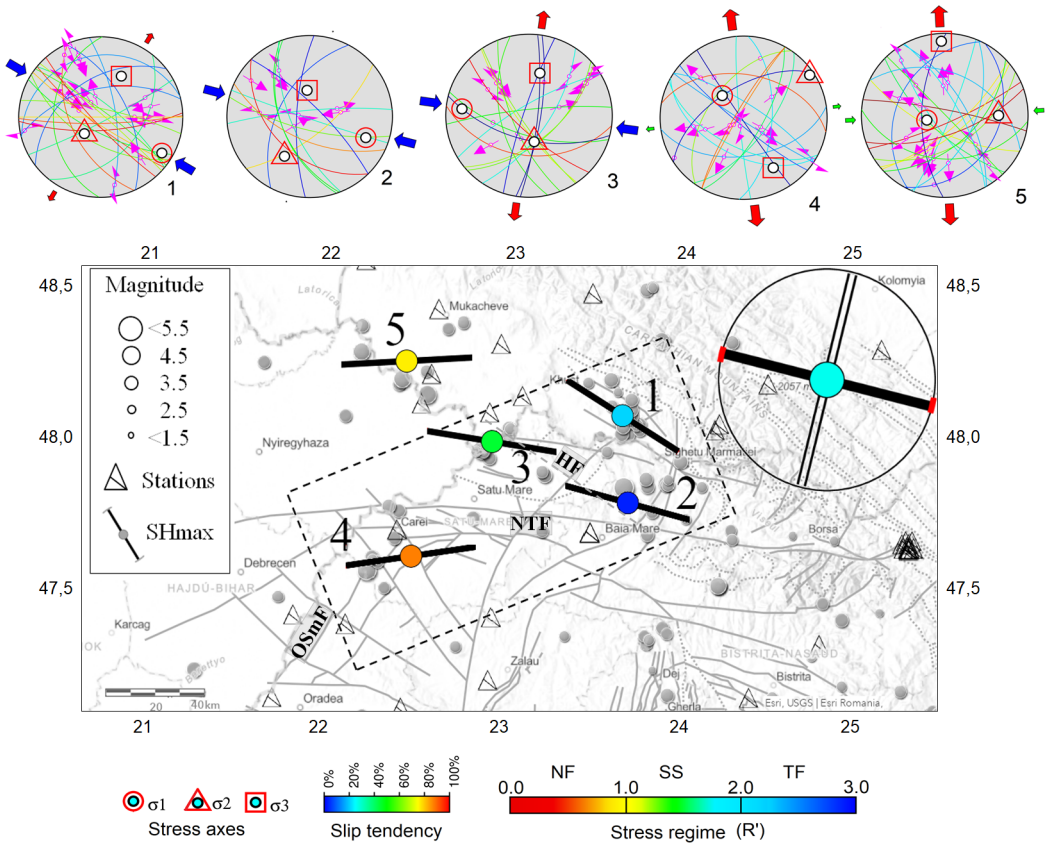

Figure 10. Stress tensor pattern for the Crisana-Maramures Seismogenic Zone (CM) (large symbol-upper right corner) and five clusters numbered with digits from 1 to 5 as in Table 2 (smaller symbols); the thick bars are SHmax (red circle arcs are standard deviation 1-sigma) and double thin lines are Shmin; the filling colours of the central circle correspond to stress regime (R′) as shown in the coloured scale (bottom). Above the map are the lower hemisphere stereo plots of nodal planes of FMS used in inversion; the resolved shear is shown by the slip-tendency, slipping direction and faulting style for NP1 (magenta double arrows are strike-slip, single arrows are normal or reverse faults). For other symbols and their explanation see Figure 9. NTF is the North Transylvanian Fault system, HM is Halmeu Fault, and OsmF is the Oradea-Satu Mare Fault system after Polonic [1985].

The highest reactivation potential (ST > 80%) is computed now for 1) normal and normal strike-slip faults oriented NE-SW and WNW-ESE to EW, respectively which border the large neotectonic grabens (cluster 4) and Transcarpathian Depression (cluster no. 5), e.g. NTF, Oradea-Satu Mare Fault [Polonic, 2005), 2) NW-SE to EW oriented strike-slip faults (clusters 1 and 3) and 3) reverse strike-slip faults on NW-SE oriented planes (cluster 2) e.g. Halmeu Fault [Polonic, 2005].

The strongest earthquake with computed FMS occurred on 30 March 1979 (47.82/23.679, Mw = 5.0, h = 12.8 km) within cluster no. 2. The faulting is strike-slip with reverse component (rake 139°) on an almost vertical plane (dip = 86.4°) oriented N110°E along the NTF system. Zsiros [2006] computed, on a macroseismic data basis, the faults azimuth for two great events that occurred in cluster no. 4 (47.5/22.3) on 01.07.1829, Mw = 5.7, Io = 7.5MSK, h = 27 km and 15.10.1834, Mw = 6.6, h = 24 km, Io = 9MSK. They are NE-SW-oriented (N76° ± 20.4° and N52.6° ± 33.9°) along with the OSmF system that controls the Galospetreu Graben [Polonic, 1985].

4.2.2 Banat Seismogenic Zone (BA)

Within the BA zone (Figure 11), the SHmax direction computed using 212 FMS, is consistent with the NE-SW-oriented smoothed stress trajectories within the eastern border of the Pannonian Depression and the direction of tectonic forces from the Africa-Europe collision area [Bada et al., 1998; 2007; Heidbach et al., 2018]. The stress regime is transtensive and the σ3-axis is stable-oriented NNW-SSE (StdDev = 21°) compared to the σ1-axis

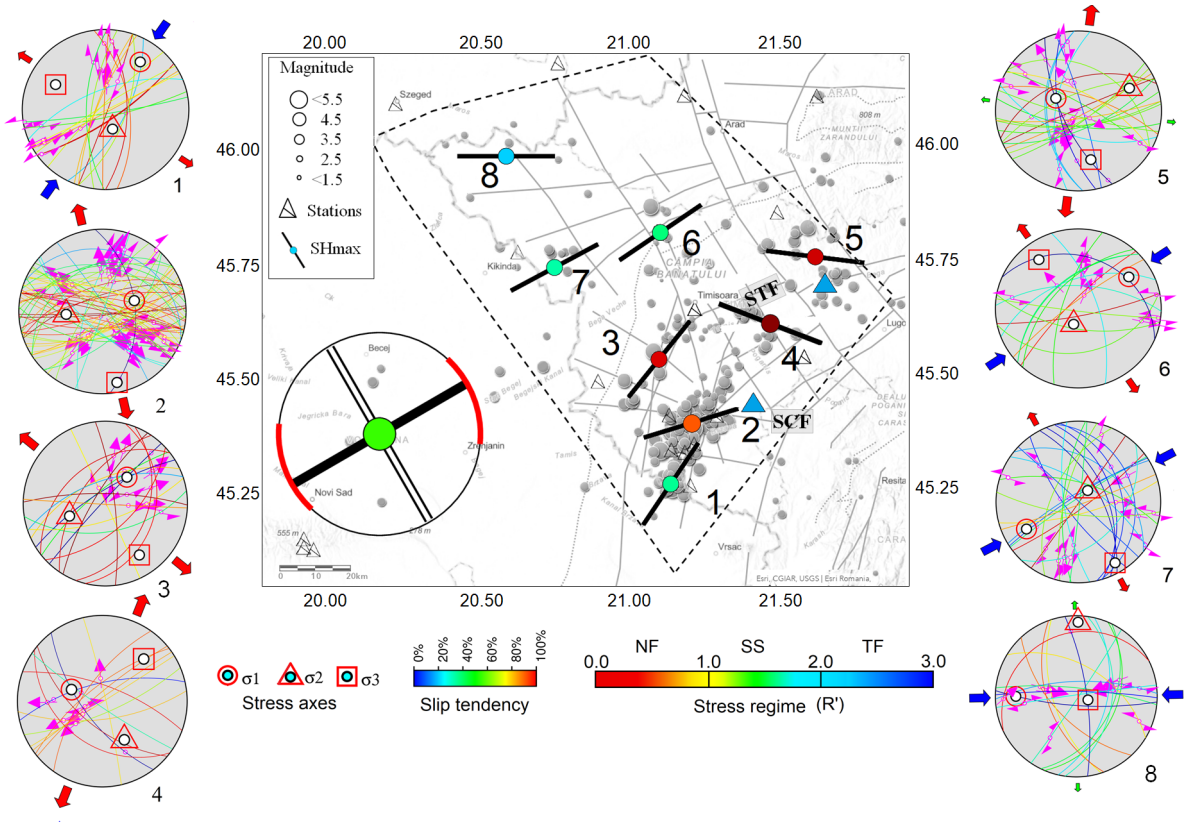

Figure 11. Map of stress tensor inversion results for Banat Seismogenic Zone (BA); blue triangles are Quaternary volcanoes. STF and SCF are South Transylvaniana and South Carpathian Fault systems. More details about symbols and scales are in Figure 10.

more unstable (StdDev = 45°). The stress regime computed by Bada et al. [2007] is strike-slip (R = 0.3), different from ours (transtensive, R = 0.85; R′ = 1.15), most likely due to the low diversity of focal mechanisms obtained for a small number of earthquakes located in a small area from southern BA. Under these stress conditions, the structures oriented NE-SW to E-W (e.g. STF, SCF) are preferably reactivated in the future (ST > 80%) while the NW-SE to NNE-SSW striking faults with low dip angles that controlled the development of the neotectonic grabens are unlikely to be reactivated (ST < 20%). Further North (BZ area), SHmax rotates counterclockwise by 33° becoming parallel to the Mid-Hungarian shear zone. Here the stress regime is transpressive to compressive with ST > 80% for NS to NE-SW-oriented faults.

To identify the stress field characteristics that could control seismogenesis on smaller particular structures, we defined 8 datasets with Nmin = 8 FMS, Nmax = 112 FMS (Figure 11) belonging to clusters located mainly on the flanks of the two neotectonic grabens defined by Polonic [1985] intersected with almost perpendicular faults. There are large differences between clusters both in terms of stress tensor orientation and in the tectonic regime. Thus, a systematic clockwise rotation of SHmax from West to East and stress regime changes from South to North can be pointed out as a consequence of the details of the geological and tectonic structure (faults, magmatic structures), which can generate important discontinuities of the stress tensor. SHmax rotates slowly from NE-SW (clusters no. 1-3) to EW (clusters no. 6-8) in the western half of the zone, and then it rotates with 90°, up to NW-SE in the East (clusters no. 4 and 5). The stress regime is extensive (clusters no. 2, 3, 4 and 5) around the area where two Quaternary volcanoes and several native deep CO2 and mineral water springs have been located [Oros, 2011; Sandulescu, 1984; Polonic; 1985 and references therein] and the SHmax rotates from NE-SW to NW-SE. It changes to a transpressive one in its southern edge (cluster no. 1) and is mainly compressive in the North (clusters no. 6, 7 and 8), while the SHmax does not change its regional direction NE-SW.

The potential fault appears to be maximum (ST > 80%) for 1) normal fault striking NW-SE and NNE-SSW to EW (clusters no. 3, 4 and 5), 2) normal strike-slip faults with EW directions, such as the SCF (cluster no. 2), 3) strike-slip faults oriented NNE-SSW to NE-SW, such as STF (cluster no. 1) and the faults that border basement

structures (clusters no. 6 and 7), 4) reverse strike-slip faults oriented NNW-SSE and EW (cluster no. 8), respectively, along with the longitudinal faults bordering neotectonic structures and the low angle faults that border basement nappes of Carpathians. The focal mechanisms computed for the strongest earthquakes are consistent with these results; e.g. strike-slip: cluster no. 1 and no. 6 (12.07.1991, Mw = 5.6, NP1azimuth = N9°; 30.08.1941, Mw = 5.2, NP1azimuth = 203°; 17.04.1974, Mw = 5.1, NP1azimuth = 173°); normal faults: cluster no. 3 (27.05.1959, Mw = 5.3, NP1azimuth = 245°; 22.10.1960, Mw = 5.1, NP1azimuth = 168°); normal strike-slip faults: cluster no. 2 (02.12.1991, Mw = 5.5, NP1azimuth = 103°).

4.2.3 Danube Seismogenic Zone (DA)

The stress tensor has been computed using 139 FMS (Figure 12). SHmax rotated clockwise from NE-SW up to NW-SE (N124° ± 47°) being consistent with the pattern of Bada et al. [1998; 2007] and perpendicular to that of Heidbach et al. [2018]. The stress regime is radial extensive with σ1 almost vertical (plunge 74°) and stable oriented toward NW (azimuth 328°, StdDev = 20°). The Shmin, as the relevant stress tensor component in regions with extensional deformation, is oriented in the direction of first-order stress (N34°) and parallel to the major faults that border internal units of Dacides (CJF) and separates the orogen from the Neogene basinal structures (WF). The ENE-WSW to ESE-WNW-oriented faults systems will be most probably reactivated as Oros [2004; 2011] concluded, too based on seismicity and seismotectonics investigations.

The stress tensor has been analyzed in detail using 7 datasets with FMS computed for clusters located along with the WF (clusters no. 4, 5 and 6) and CJF (clusters no. 1, 2 and 3). We also used data from outside the area, on the western flanks of the structures identified inside the investigated area (cluster no. 7). The regional stress

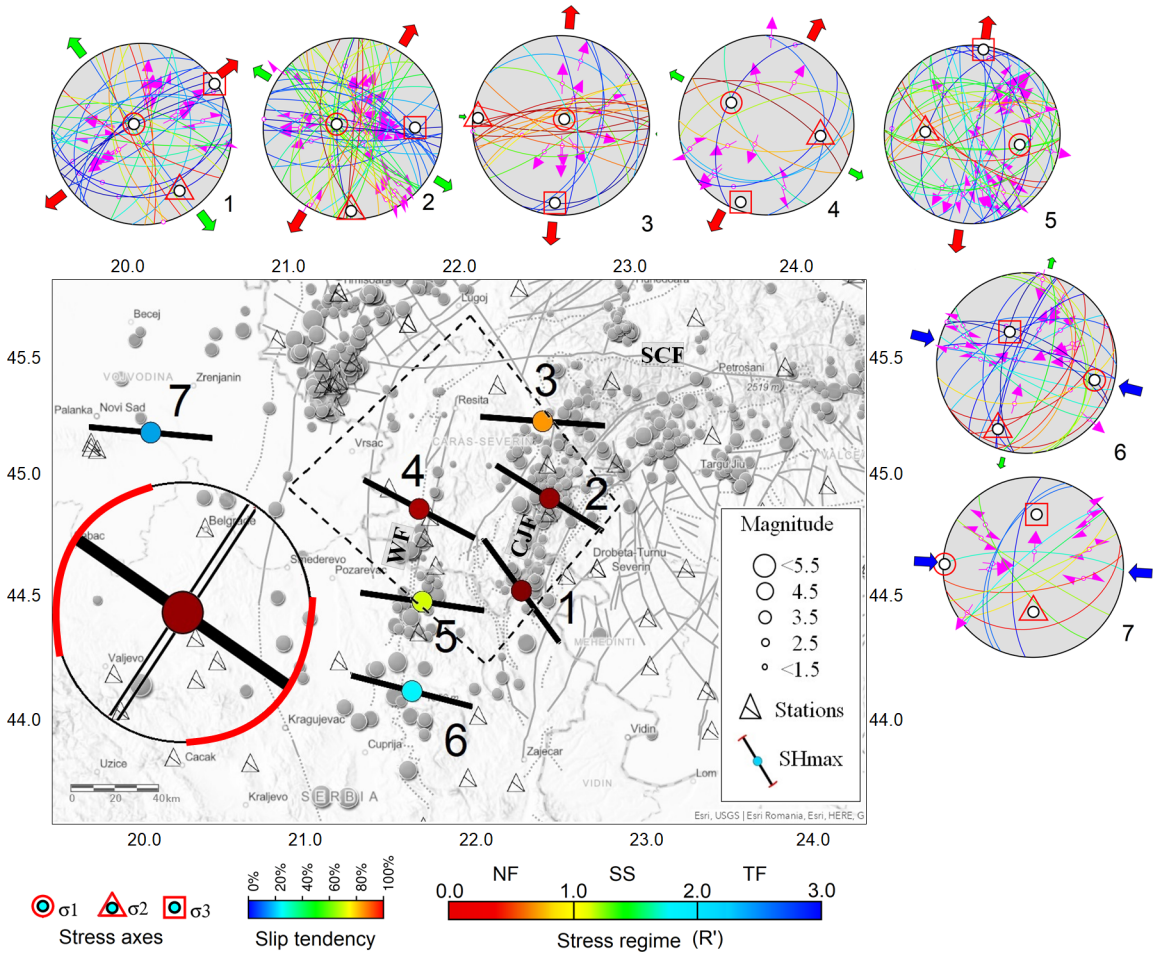

Figure 12. Map of stress tensor inversion results for Danube Seismogenic Zones (DA). WF is the Western Fault system and SCF is the South Carpathian Fault system. More details about symbols and scales are in Figure 10.

pattern changes from West to East. SHmax rotates clockwise from NE-SW to EW and WNW-ESE in the western and southwestern edges of the zone (clusters no. 4, 5 and 6) parallel to SCF (cluster no. 7) and perpendicular to the mountain chain bordered by WF. The tectonic stress regime changes from transpressive (clusters no. 6 and 7) to the transtensive (cluster no. 5) and radial extensive (cluster no. 4). The NNE-SSW to NE-SW low angle faults (cluster no. 6) and EW-oriented structures (cluster no. 7) have the highest reactivation potential (ST > 80%) as reverse and strike-slip/normal strike-slip faults, respectively depending on their geometry. The eastern areas where the clusters are located along the Cerna-Jiu Fault system display radial extensive (clusters no. 1 and 2) and transtensive (cluster no. 3) stress conditions with SHmax changing its perpendicular to CJF direction in South (N143°E ± 20° cluster no. 1) to EW in North (N94°E10°, cluster no. 3), parallel to SCF. The NNW-SSE- up to NNE-SSW-oriented structures can be reactivated as normal and strike-slip with large normal components faults in the central and southern parts (clusters no. 1 and 2). In North (cluster no. 3), the EW-oriented structures can most likely be reactivated as normal faults. The FMS computed for the last major events and macroseismic data confirm some of these estimations. Thus, the strongest earthquakes in the DA zone (18.07.1991, Mw = 5.6) occurred within the cluster 2 area on NE-SW oriented normal fault (strike 75°, dip 52°, rake –124°) along the CJF system. The faults reactivated during the seismic sequence of 1879-1880 in the area of clusters 4 and 5 are oriented approximately NNW-SSE, parallel to WF, as it can be inferred from the elongation of the maximum intensity isoseismals [Atanasiu, 1961; Oros, 2011].

4.2.4 Fagaras-Campulung Seismogenic Zone

The FC zone exhibits a pattern of the stress field characterized by the same extensive tectonic stress regime as the DA zone, but SHmax is oriented in a perpendicular direction, consistent with the first-order stress predicted by Heidbach et al. [2018] (Figure 9). It was obtained through the inversion of 127 FMS. Faults oriented on average in the EW direction, which represent segments of the SCF, can most likely be reactivated in the future (Figure 9). Along these faults and at their intersection with IMF, 4 clusters were identified and on their basis were defined subsets of representative data for the detailed investigation of the stress state and seismotectonic characteristics (Figure 13).

SHmax rotates clockwise by 95°, from NNE-SSW in the West (N32°E ± 7°, cluster no. 1) to NNW-SSE in the East (cluster no. 4), reaching parallel with IMF. The transtensive stress regime characteristic in the West (clusters no. 1 and 2) becomes pure strike-slip in the East (clusters no 3 and 4). The normal and strike-slip with normal component faults oriented NNE-SSW and NE-SW have the highest values of the slip-tendency in the West (clusters no. 1 and 2). To the East, the situation is changing significantly, the structures oriented towards NNW-SSE, NW-SE, EW and NS have a high probability of reactivation as strike-slip faults. The focal mechanism of the strongest earthquake that occurred within the cluster 3 area (26.01.1916, Mw = 6.4) corresponds to dextral normal strike-slip faulting (rake –155°) with the rupture plane most probable oriented WNW-ESE (N284°), as constrained by the tectonic (SCF) and macroseismic data [Atanasiu, 1961; Oros et al., 2019b].

4.2.5 Transylvania Seismogenic Zone (TR)

Earthquakes with focal mechanisms in the TR zone are very few and scattered throughout its surface, without well-defined clusters, so the state of stress is computed, analyzed and discussed on a 13 FMS basis (Figure 9). SHmax is stable and oriented N37°E ± 9° on the first-order stress direction of Heidbach et al. [2018]. A very good correlation is also noted between the orientation of the σ1-axis in our model and the results obtained by Muller et al. [2010] and by Zugravescu et al. [2005; 2010] who used borehole data. The tectonic regime is a pure strike-slip with the T-axis oriented almost invariably in the NW direction. The NE-SW-oriented faults (e.g. PTF) have the highest probability to be reactivated (ST > 80%).

4.2.6 Central-South Carpathian Zone (CSC)

Between DA and FC zones, there is an area where high recent seismic activity was recorded [Oros, 2011; Placinta et al., 2016], which we call here the Central-South Carpathians zone (Figure 14). It can be described as a hazard seismic source considering the strong earthquakes known so far on the SCF (19.01.1665, 45.504/22.647, Mw = 5.0;

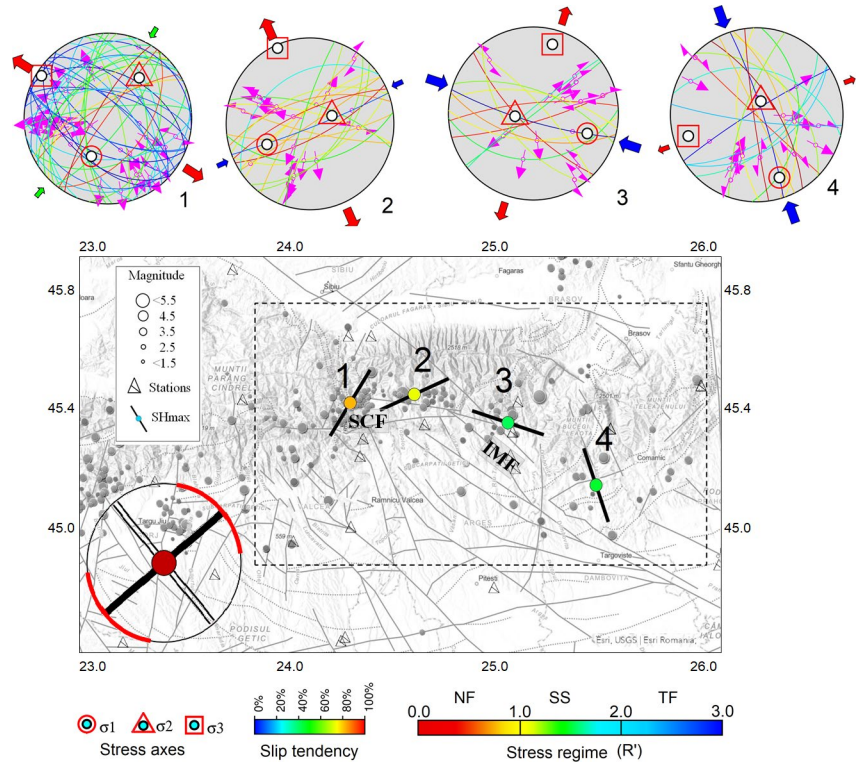

Figure 13. Map of stress tensor inversion results for Fgaras-Campulung Seismogenic Zone (FC). SCF is the South Carpathian Fault system, and IMF is the Intra-Moesian Fault system. More details about symbols and scales are in Figure 10.

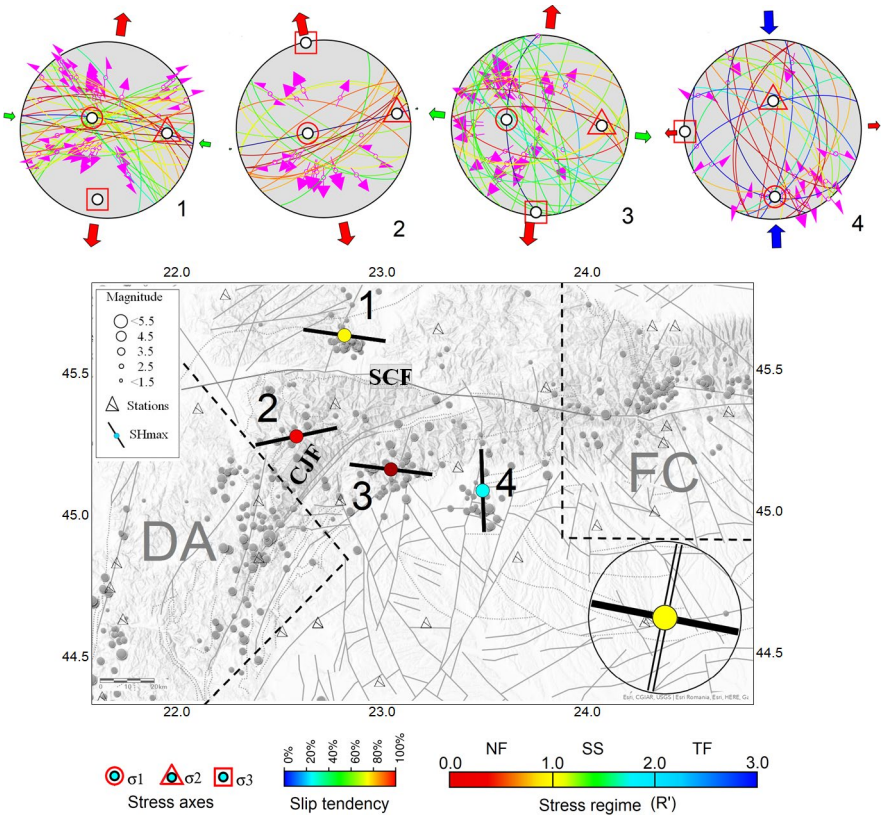

Figure 14. Map of stress tensor inversion results for the central area of the South Carpathians (CSC). SCF is the South Carpathian Fault system, and CJF is the Cerna-Jiu Fault system. More details about symbols and scales are in Figure 10.

09.07.1912, 45.592/22.894, Mw = 5.2) and at the orogen-Moesian Platform contact (20.06.1643, 45.0/23.0, Mw = 5.2) [Oros, 2011]. The stress tensor pattern and faulting style computed by the inversion of 144 FMS are comparable with those of the North of the DA zone (Figures 9 and 14). SHmax is oriented parallel to the SCF system that can be most likely reactivated in the future and the stress regime is transtensive (extensive strike-slip). At the local scale (Figure 14), the stress field computed for the 4 clusters displays 1) extensional faultings in the orogen structures with almost invariable NS-oriented Shmin (clusters no. 1-3) and 2) compressional faulting/transpressive stress regime at the contact between the Carpathians and Moesian Platform (cluster 4) with constant NS-oriented (StdDev = ± 14°). Faults belonging to the SCF and CJF systems are most likely to be reactivated as normal and normal strike-slip faults while faults oriented on average NS in the cluster 4 area will most likely be reactivated as strike-slip faults.

4.2.7 Eastern Carpathians (EC) area

Within the Eastern Carpathians area (EC) a pure compressive stress field with almost vertical σ3-axis and SHmax-oriented NW-SE is characteristic and can be well correlated with the model computed by Muller et al. [2010] in the northern half of the orogen (Figure 9). The stress tensor inversion was based on 49 FMS. The ST > 80% is computed for the low-angle faults oriented on widely variable directions, characteristic of Neogene volcanism areas (Figure 9).

5. Conclusions

We elaborated a new, significantly improved, seismological database containing focal mechanisms that cover the Intra-Carpathian region of Romania. It contains 1217 focal mechanism solutions with qualities from A to D. The superiority of our catalogue over the others developed up to the present consists of the:

i) the source parameters of the earthquakes, such as location and moment magnitude, have been (re)computed on a revised primary data basis,
ii) the focal mechanism solutions have been computed using both polarities and S/P ratios measured on the original records,
iii) the parameters of mechanisms are associated for the first time with quality indicators that reflect the robustness and stability of the solutions,
iv) the catalogue extends the limit of the Romanian database until the early instrumental period (1909-1980) and uses digitized historical seismograms to apply the full waveforms inversion methods,
v) the high spatial resolution of the A and B quality FMS both at the level of large structures (tectonic blocks, fault systems) and the scale of individual faults defined by seismic sequences,
vi) for the first time in a Romanian catalogue of mechanisms, there were estimated errors in the nodal planes and a quality index was assigned for each mechanism in agreement with international practice.

Using our catalogue we emphasized the strong heterogeneity of the stress field in the region reflected in the orientation of the S1 axis and tectonic regime. This heterogeneity resulted from strong interferences of regional and local sources as different authors already mentioned [e.g. Bada et al., 1998; 2007; Muller et al., 2010].

The seismically active faults are oriented generally in the direction of faults systems that border or cross the major structures and geotectonic units. These have been reactivated in a transtensive to extensive stress regimes in the western and southern sectors of the region (FST, FSC, FNT in the West and WF, CJF, SCF in the South) and a transpresive stress regime in the northeastern sector (the low-angle faults of the East Carpathians and PTF at the contact between Transylvanian Basin and Apuseni Mountains).

Variations in the tectonic regime pattern and the orientation of stress tensor axes, including slipping tendencies, show very different trends from one seismogenic zone to another, suggesting the reaction of a complex geological environment to the action of a regional stress field disturbed by the strongest local sources.

Acknowledgements. This paper was carried out within Nucleu Program MULTIRISC, projects no PN19080101 and PN19080102 supported by the National Authority for Scientific Research and Innovation of Romania. The authors are grateful to the anonymous reviewers for their comments and useful suggestions.

References

Aki, K. and P. G. Richards (1980) Quantitative Seismology, Theory and Methods, I and II v., W.H. Freeman (Editor), San Francisco.

Allmann, B. P., P M. Shearer and E. Hauksson (2008). Spectral Discrimination between Quarry Blasts and Earthquakes in Southern California, Bull. Seism. Soc. Am., 98, 4, 2073-2079.

Angelier, J. and P. Mechler (1977). Sur une methode graphique de recherche des contraints principales egalement utilisable en tectonique et en seismologie: la methode des diedres droits, Bulletin de la Société Géologique de France, 7, 19, 1309-1318.

Atanasiu, I. (1961). The earthquakes from Romania (in Romanian), Romanian Academy Publishing House, 194, Bucharest, Romania.

Bada, G., S Cloetingh., Gerner P and F. Horvath (1998). Sources of recent tectonic stress in the Pannonian region: inferences from finite element modelling, Geophys. J. Int., 134, 1, 87-101.

Bada, G., F. Horváth, P. Dövényi, P. Szafián, G. Windhoffer and S. Cloetingh (2007). Present-day stress field tectonic inversion in Pannonian Basin, Global Planet. Change, 58, 165-180.

Bala, A., M. Radulian, and E. Popescu (2003). Earthquakes distribution and their focal mechanism in correlation with the active tectonic zones of Romania, J. Geodyn., 36, 129-145.

Bala, A., V Raileanu, Dinu C and M. Diaconescu (2015). Crustal seismicity and active fault systems in Romania, Romanian Rep. Phys., 67, 3, 1176-1191.

Bala, A., D.Toma-Danila and M. Radulian (2019). Focal mechanisms in Romania: statistical features representative for earthquake-prone areas and spatial correlations with the tectonic province, Acta Geodaetica et Geophysica, 54, 1, doi: 10.1007/s40328-019-00260-w.

Bouchon, M. (1981). A simple method for calculating Green's functions for elastic layered media, Bull. Seismol. Soc. Am., 71, 959-972.

Celerier, B. (2008). Seeking Anderson's faulting in seismicity: a centennial celebration, Rev. Geophys., American Geophysical Union, 46, 4, RG4001; doi.org/10.1029/2007RG000240.

Cornea, I., G. Polonic and V. Steflea (1980). Seismotectonic studies in Baia Mare-Halmeu area, Studii si Cercetari de Geologie, Geofizica, Geografie, Geofizica, 19-52, 60.

Delvaux, D., R. Moyes, G. Stapel, C. Petit, K. Levi, A. Miroshnichenco, V. Ruzhich and V. Sankov (1997). Paleostress reconstructions and geodynamics of the Baikal region, Central Asia, Part 2. Cenozoic rifting, Tectonophysics, 282, 1-38.

Delvaux, D. and B. Sperner (2003). Stress tensor inversion from fault kinematic indicators and focal mechanism data: the tensor program, In New Insights into Structural Interpretation and Modelling D. Nieuwland (Editor), Geol. Society, London, Spec. Pub., 212, 75-100.

Delvaux, D. and A. Barth (2010). African stress pattern from formal inversion of focal mechanism data, Tectonophysics, 482, 105-128.

Diehl, T. and E. Kissling (2007). Users Guide for consistent phase picking at local to regional scales, Institute of Geophysics, (Appendix C of PhD Thesis of T. Diehl), Technical Report, ETH Zurich, 21, http://mercalli.ethz.ch/~tdiehl/Data2Download/Pickguide_v1.2.1.pdf.

Duputel, Z., L. Rivera, Y. Fukahata and H. Kanamori (2012). Uncertainty estimations for seismic source inversions, Geophys. J. Int., 190, 1243 - 1256.

Ferrari, G. and N.A. Pino (2003). Euroseismos 2002-2003 a project for saving and studying historical seismograms in the Euro-Mediterranean area, Geophys. Res. Abstr., 5, EAE03-A-05274, http://adsabs.harvard.edu/abs/2003EAEJA, 5274F.

Fossen, H. (2010). Structural Geology. Cambridge University Press, Cambridge, 463, doi.org/10.1017/CBO9780511777806.

Giardini, D., S. Wiemer, D. Fah and D. Deichmann (2004). Seismic Hazard Assessment of Switzerland. The report, Swiss Seismological Service, ETH Zurich, 88, http://www.seismo.ethz.ch/export/sites/sedsite/knowledge/.galleries/pdf_hazard2004/hazard_report_2004.pdf_2063069299.pdf.

Heidbach, O. (2016). WSM quality ranking scheme, database description and analysis guidelines for stress indicator, WSM Scientific Technical Report, WSM STR 16-01, Available at http://www.world-stress-map.org/data.

Heidbach, O., Rajabi M., Cui X., Fuchs K., Muller B., Reinecker J., Reiter K., Tingay M., Wenzel F., Xie Fand O. Ziegler (2018). The World Stress Map database release 2016: Crustal stress pattern across scales, Tectonophysics, 744, 2018, 484-498.

Hardebeck, J. L. and E. Hauksson (2001). Crustal stress field in southern California and its implications for fault mechanics, J. Geophys. Res., 106, B10, 21859-21882.

Hardebeck, J. L. and P.M. Shearer (2002). A new method for determining first-motion focal mechanisms, Bull. Seismol. Soc. Am., 92, 2264-2276.

Hardebeck, J. L. and P.M. Shearer (2003). Using S/P amplitude ratios to constrain the focal mechanisms of small earthquakes, Bull. Seism. Soc. Am., 93, 2434-2444.

Khattri, K. (1973). Earthquake focal mechanism studies, Earth-Science Reviews, 9, 19-63.

Kilb, D. and J.L. Hardebeck (2006). Fault parameter constraints using relocated earthquakes: A validation of first-motion focal-mechanism data, Bull. Seism. Soc. Am., 96, 1140-1158.

Kisslinger, C., J.R. Bowmann and K. Koch (1981). Procedures for computing focal mechanisms from local (SV/P)z data, Bull. Seism. Soc. Am., 71, 6, 1719-1729.

Kulhánek, O. (2002). The structure and interpretation of seismograms. In: Lee, W. H. K., Kanamori, H., Jennings, P. C., and Kisslinger, C. (Eds.) (2002). International Handbook of Earthquake and Engineering Seismology, Part A. Academic Press, Amsterdam, 333-348.

Lin, G. and P. G. Okubo (2016). A large refined catalogue of earthquake relocations and local mechanisms for the Island of Hawai and its seismotectonic implications, J. Geophys. Res.: Solid Earth, 121, 5031-5048, doi:10.1002/2016JB013042.

Linzer, H-G, W. Frisch, P. Zweigel, R. Girbacea, H-P Hann and F. Moser (1998). Kinematic evolution of the Romanian Carpathians, Tectonophysics, 297, 133-156.

Malagnini, L., R.B. Herrmann and K. Koch (2000). Regional Ground-Motion Scaling in Central Europe, Bull. Seismol. Soc. Am., 90, 4, 1052-1061.

Malita, Z. and F. Radulescu (2010). Focal mechanisms of some crustal earthquakes that occurred in the Pannonian Depression (Arad-South Timisoara area), the Moesian Platform and North-Dobrogean orogen, Revue Roumaine de Géophysique, 54, 19-37.

Michael, A.J. (1984). Determination of stress from slip data: Faults and folds, J. Geophys. Res., 89, 11, 517-11, 526.

Michael, A.J. (1987). Use of focal mechanisms to determine stress: a controlled study, J. Geophys. Res., 92, 357-368.

Michael, A. J., W.L. Ellsworth and D. Oppenheimer (1990). Co-seismic stress changes induced by the 1989 Loma Prieta, California earthquake, Geophys. Res. Lett., 17, 1441- 1444.

Michelini, A., B. De Simoni, A. Amato and E. Boschi (2005). Collecting, digitizing and distributing historical seismological data, EOS Trans. AGU, 12 July 2005, 28/86.

Muller, B., Heidbach O., Negut M, Sperner B and T. Buchmann (2010). Attached or not attached: Slab dynamics beneath Vrancea, Romania, Tectonophysics, 482, 1-4, 139-149.

Oncescu, M. C., V. Marza, M. Rizescu and M. Popa (1999). The Romanian earthquakes catalogue, 984-1997. In Vrancea Earthquakes: Tectonics, Hazard Risk Mitigation; Wenzel Lungu (Editors), Kluwer Publication, pp. 43-47, and continuously updated on www.infp.ro.

Oros, E. (2003). Banat Seismic Network (Romania). Evolution and performances, Studii si Cercetari de Geofizica, 41, 112-125.

Oros, E. (2004). The April-August 2002 Moldova Nouă earthquakes sequence and its seismotectonic significance, Revue Roumaine de Geophysique, 48, 49-68.

Oros, E., M. Popa and I.A. Moldovan (2008). Seismological DataBase for Banat Seismic Region – Part 1: The Parametric Earthquake Catalogue, Romanian J. Phys., 53, 7-8, 955-964.

Oros, E., M. Popa, I.A. Moldovan and E. Popescu E. (2008). Seismological DataBase for Banat Seismic Region (Romania). Part 2: The Catalogue of the Focal Mechanism Solutions, Romanian J. Phys., 53, 7-8, 965-977.

Oros, E. (2011). Research on seismic hazard for the seismic region of Banat (Romania), PhD Thesis (in Romanian), University of Bucharest.

Oros, E. (2013). Analysis of two earthquake sequences that occurred in 2012 in the Timisoara area, Romania, Romanian J. Phys., 58, 7-8.

Oros, E. and M. Diaconescu (2014). Recent vs Historical seismicity analysis for Banat Seismic Region (western part of Romania), In Proceedings of the 5th National Conference on Earthquake Engineering and the 1st National Conference on Earthquake Engineering and Seismology, 1, 181-189, Conspress Publishing, Bucharest.

Oros, E., M. Popa, C. Ghita, M. Rogozea, A. Rau-Vanciu and C. Neagoe (2016). Catalogue of focal mechanism solutions for crustal earthquakes in Intra-Carpathian region of Romania, Paper presented at the 35th General Assembly of the European Seismological Commission, 4-11 September 2016, Trieste, Italy, ESC2016-142.

Oros, E., M. Popa and M. Rogozea (2017). Calibration of crustal historical earthquakes from Intra-Carpathian region of Romania, 95, 032004, doi:10.1088/1755-1315/95/3/032004.

Oros, E., M. Popa and M. Diaconescu (2018). The Seismogenic Sources from the West and South-West of Romania. In: Vacareanu R., Ionescu C. (Ed.) Seismic Hazard and Risk Assessment, Springer Natural Hazards, Springer International Publishing AG, Book: Seismic Hazard and Risk Assessment, Cap. Seismicity Analysis, 53-69, doi.org/10.1007/978-3-319-74724-8_4.

Oros, E., A. O. Placinta and M. Popa (2019). Calibration and validation of the MEEP method for location and magnitude estimation of historical earthquakes from Intra-Carpathian region of Romania, Proceedings WMESS 2018, IOP Conference Series Earth and Environmental Science, 221, 012057, doi: 10.1088/1755-1315/221/1/012057

Oros, E., E. Constantinescu, D. Paulescu, M. Popa and A.O. Placinta (2019). Using early instrumental data to determine the source parameters of the strongest historical earthquakes that occurred in West Romania (1900-1980), Proceedings SGEM 2019, Sci. Tech. Geol., Explor. Mining, 1.1, 19, 991-998, doi: 10.5593/sgem2019/1.1.

Oros, E., A.O. Placinta, M. Popa, M. Rogozea and D. Paulescu (2019). Attenuation of macroseismic intensity for crustal Romanian earthquakes: calibrating the Bakun-Wentworth's method, Proceed.WMESS, IOP Conference Series Earth and Environmental Science.

Ottemoller, L., P. Voss and J. Havskov (2021). Seisan earthquake analysis software for windows, solaris, linux and MacOSX, Version 12.0, University of Bergen, ISBN 978-82-8088-501-2, 607.

Paulescu, D., M. Rogozea, M. Popa and M. Radulian (2016). Digitized Database of Old Seismograms Recorder in Romania, Acta Geophysica, 64, 4, 963-977.

Pintore, S., M. Quintiliani and D. Franceschi (2005). Teseo: a vectorized of historical seismograms, Compu. Geosci., 31, 10, 1277-1285.

Placinta, A. O., E. Popescu, F. Borleanu, M. Radulian and M. Popa (2016). Analysis of source properties for the earthquake sequences in the South-Western Carpathians (Romania), Romanian Rep. Phys., 68, 3, 1240-1258.

Polonic, G. (1985). Neotectonic activity at the eastern border of the Pannonian Depression and its seismic implications, Tectonophysics, 47, 109-115.

Polonic, G., D. Zugravescu and V. Negoita (2005). The present-day stress field pattern in the eastern Carpathian bend area, Revue Roumaine de Geophysique, 49, 3-30.

Popa, M., M. Radulian, D. Ghica, C. Neagoe and E. Nastase E (2015). Romanian seismic network from 1980 to the present, Springer Proceedings in Physics, 163, 117-132.

Popa, M., I. Munteanu, F. Borleanu, E. Oros, M. Radulian and C. Dinu (2018). Active tectonic deformation and associated earthquakes. A case study: South Carpathians Bend zone, Acta Geodaetica and Geofisica, 53, 1-2, 1-19, doi: 10.1007/s40328-018-0224.

Pujol, J. (2000). Joint Event Location – The JHD Technique and Applications to Data from Local Seismic Networks. In: Thurber C.H., Rabinowitz N. (Editors) Advances in Seismic Event Location, Modern Approaches in Geophysics,18, Springer, Dordrecht.

Radulescu, F. (2009). Romanian seismology – historical, scientific and human landmarks, Revue Roumaine de Géophysique, 52-53, 101-121.

Radulian, M., N. Mandrescu, E. Popescu, A. Utale and G.F. Panza (1996). Seismic activity and stress field characteristics for the seismogenic zones of Romania, International Centre for Theoretical Physics, IC/96/256, http://streaming.ictp.it/preprints/P/96/256.pdf.

Radulian, M., N. Mandrescu, E. Popescu and A. Utale (1999). Seismic activity and stress field in Romania, Romanian J. Phys., 44, 9-10, 1051-1069.

Radulian, M., N. Mandrescu, G.F. Panza, E. Popescu and A. Utale (2000). Characterization of Seismogenic Zones of Romania, Pure Appl. Geophys., 157, 57-77.

Radulian, M., E. Popescu, A. Bala and A. Utale (2002). Catalogue of fault plane solutions occurred on the Romanian Territory, Romanian J. Phys., 47, 5-6, 663-685.

Radulian, M., A. Bala, E. Popescu and D. Toma-Danila (2018). Earthquake mechanism and characterization of seismogenic zones in the south-eastern part of Romania, Ann. Geophys., 61, 1, SE108, doi: 10.4401/ag-7443.

Reasenberg, P. and D. Oppenheimer (1985). Fpfit, fpplot, and fppage: Fortran computer programs for calculating and displaying earthquake fault plane solutions, Technical reports, U.S. Geol. Survey, doi:10.3133/ofr85739.

Ren, Y., B. Grecu, G. Stuart, G. Houseman, and E. Hegedus (2013) South Carpathian Project Working Group Crustal structure of the Carpathian-Pannonian region from ambient noise tomography, Geophys. J. Int., 195, 1351-1369.

Sandulescu, M. (1984). Geotectonics of Romania (in Romanian), The Academy's Publishing House, Bucharest, 450.

Schmid, S. M., B. Bernoulli, B. Fugenschuh, L. Matenco, S. Schefer, R. Schuster, M. Tischler and K. Ustaszewski (2008). The Alpine-Carpathian-Dinaridic orogenic system: correlation and evolution of tectonic units, Swiss J. Geosci., 101, 139-183.

Sokos, E. N. and J. Zahradnik (2008). ISOLA a Fortran code and a Matlab GUI to perform multiple-point source inversion of seismic data, Compu. Geosci., 34, 8, 967-977.

Snoke, J. A., J.W. Munsey, A.G. Teague and G.A. Bollinger (1984). A program for focal mechanism determination by the combined use of polarity and SV-P amplitude ratio data, Earthquake notes, 55.

Sperner, B., D. Ioane and R.J. Lillie (2004). Slab behaviour and its surface expression: new insights from gravity modelling in the SE-Carpathians, Tectonophysics, 382, 51-84.

Toth, L., P. Mónus, M. Kiszely and D. Trosits (2018). Hungarian Earthquake Bulletin, GeoRisk, Budapest, 140, doi:10.7914/SN/HM.

Ursino, A., H. Langer, L. Scarfi, G. Di Grazia and S. Gresta (2001). Discrimination of quarry blasts from tectonic microearthquakes in the Hyblean Plateau (Southeastern Sicily), Annali di Geofisica, 44, 4, 703-722.

Wiemer, S. (2001). A software package to analyze seismicity: ZMAP, Seismol. Res. Lett., 92, 373-382.

Yang, W., E. Hauksson and P.M. Shearer (2012). Computing a Large Refined Catalogue of Focal Mechanisms for Southern California (1981-2010): Temporal Stability of the Style of Faulting, Bull. Seism. Soc. Am., 102, 3, 1179-1194, doi: 10.1785/0120110311.

Zsiros, T. (2006). Ermellek seismic source zone. Acta Geod. Geoph. Hung., 41, 2, 237-247.

Zoback, M. L. (1992). First- and second-order patterns of stress in the lithosphere: The World Stress Map Project, J. Geophys. Res., 97, 11703-11728.

Zugravescu, D. and G. Polonic (1997). Geodynamic compartments and present-day stress state on the Romanian territory, Revue Roumaine de Geophysique, 41, 3-24.

Zugravescu, D., Polonic G.and V. Negoita (2005). The present state of stress determination in the Transylvanian basin using boreholes measurements, Studii si cercetari de Geofizica, 43, 3-14.

Zugravescu, D. and V. Negoita (2010). Earth's upper crust regime of stresses inferred from borehole measurements on the Romanian territory, Revue Roumaine de Geophysique/Romanian Geophys. J., 54, 55-64.

Data and sharing resources. The historical seismograms (raster images) used in this study were collected from the NIEP archive (www.archive.infp.ro; last accessed January 2018) and as part of the EuroSeismos project (http://storing.rm.ingv.it/es_web; last accessed January 2019) that are stored in the Sismos database (http://seismogramrequest.rm.ingv.it; last accessed January 2019).

The historical seismic bulletins and instrumental constants used in this study were collected as part of the EuroSeismos project (http://storing.rm.ingv.it/es_web; last accessed January 2019)

The recent seismicity data used in this study is available from the Romanian parametric database (http://www.infp.ro/data/romplus.txt; last accessed January 2019) and from ISC (https://doi.org/10.31905/D808B830; last accessed January 2019).

Digital Seismograms used in this study were taken from the database of NIEP, National Data Center and can be requested at this address http://www.infp.ro/.

The free software used in this paper is Teseo (https://github.com/INGV/teseo2), Seisan (ftp://ftp.geo.uib.no/pub/seismo/SOFTWARE/SEISAN/), Win-Tensor (http://DamienDelvaux.be/Tensor/WinTensor), Zmap (http://www.seismo.ethz.ch/en/research-and-teaching/products-software/software/ZMAP/), ISOLA (http://geo.mff.cuni.cz/~jz/for_ISOLAnews).

***CORRESPONDING AUTHOR: Eugen OROS**,
National Institute for Earth Physics, Calugareni, Magurele, Ilfov, Romania
e-mail: eugenoros@gmail.com and eugeno@infp.ro